Model Catalyst Approaches from Support and Active Species for Understanding of Ziegler-Natta Catalysis

KEISUKE GOTO

Japan Advanced Institute of Science and Technology

Model Catalyst Approaches from Support and Active Species for Understanding of Ziegler-Natta Catalysis

by

KEISUKE GOTO

Submitted to
Japan Advanced Institute of Science and Technology
In partial fulfillment of the requirements
For the degree of
Doctor of Philosophy

Supervisor: Professor Dr. Minoru Terano

School of Materials Science

Japan Advanced Institute of Science and Technology

March 2014

Referee-in-chief: **Professor Dr. Minoru Terano**
Japan Advanced Institute of Science and Technology

Referees: **Professor Dr. Goro Mizutani**
Japan Advanced Institute of Science and Technology

Associate Professor Dr. Tatsuo Kaneko
Japan Advanced Institute of Science and Technology

Associate Professor Dr. Toshiaki Taniike
Japan Advanced Institute of Science and Technology

Professor Dr. Hisayuki Nakatani
Kitami Institute of Technology

Preface

The present dissertation is the result of the studies under the direction of Professor Dr. Minoru Terano during 2011-2014. The purpose of this dissertation is to develop new type of Ziegler-Natta model catalyst based on active sites and support structural design. The first chapter is a general introduction according to the object of this research. Chapter 2 describes the control of active site structure and polymerization properties of $MgCl_2$-supported titanocene catalysts. Chapter 3 describes the UHV preparation of $MgCl_2$ active surface for Ziegler-Natta model catalyst. The last chapter summarizes the conclusive items of this dissertation.

Keisuke Goto

Terano Laboratory,

School of Materials Science,

Japan Advanced Institute of Technology

Contents

Chapter 1

General Introduction

1.1 Introduction

The market for polyolefin is one of the biggest chemical business field in the world. The amount of production of polyolefin has been increasing each year with the enlargement in a demand of that. The world's total annual production of polyolefin reached over one hundred million tons in 2005, and an average annual growth rate in production of polyolefin is expected to be 5% by 2011. It was also suggested that the growth rate would be likely to maintain even in a distant future [1]. This huge market based on the various technologies for polymer synthesis including catalyst chemistry. Isotactic polypropylene is produced by heterogeneous Ziegler-Natta catalysts and homogeneous organic metal complexes, especially IV group metallocene catalysts. $MgCl_2$-supported Ziegler-Natta catalyst consists of $TiCl_4$, $MgCl_2$, donors, triethylaluminum and H_2. Ziegler-Natta catalysts are characterized with multiple active sites to produce polydisperse polymer. On the other hand, organometallic polymerization catalysts have the single-site nature to give monodisperse polymer, allowing a clear correlation between structure of active site and structure of PP. However, industrial production of PP has been performed with Ziegler-Natta catalysts, owing to its high stability and capability of producing PP with a higher melting point, easier processability, and better morphology.

1.2 Chemistry of $MgCl_2$-Supported Ziegler-Natta Catalyst

The industrial process of stereospecific polymerization of propylene is performed with heterogeneous Ziegler-Natta catalysts, in which the active site consists of titanium atoms, bonded to

the growing polymer chain, placed on the sides of structural layers of $TiCl_3$ or $MgCl_2$ layer compounds [2]. The finding that $MgCl_2$, mechanically or chemically activated, behaves as an ideal support for the fixation of titanium chlorides opened a new era in the field of Ziegler-Natta catalysed polymerization, both from an industrial standpoint and from a scientific point of view.

The key to the success of $MgCl_2$ as a support is the crystal structure, which is very similar to that of $TiCl_3$ with respect to interatomic distances and crystal forms. Anhydrous $MgCl_2$ is a solid, which possesses a typical layer structure (Fig 1.1). The atoms are organized in two-dimensional hexagonal arrays (with repetition periods a = b = 3.64 Å, $\gamma = 120^\circ$ for $MgCl_2$), which constitute "structural (triple) layers" [3]. In these structural layers, the magnesium atoms are sandwiched between two layers of chorine atoms, to which the magnesium atoms are octahedrally coordinated and strongly bonded. Regarding the structure of $MgCl_2$ it has been indicated by Giannini [4] that the $MgCl_2$ crystallites are made of lateral cleavage surfaces where magnesium atoms are coordinated by 4 or 5 chlorine atoms, in place of 6 chlorine atoms in the bulk of the crystal. These tetra and pentacoordinate Mg atoms are present on the (110) and (100) lateral cuts of $MgCl_2$. Upon addition of the cocatalyst (AlR_3), Ti^{4+} species ($TiCl_4$) coordinated such unsaturated surfaces is reduced to Ti^{3+} and a Ti–C bond is formed that is essential for the insertion of the monomer.

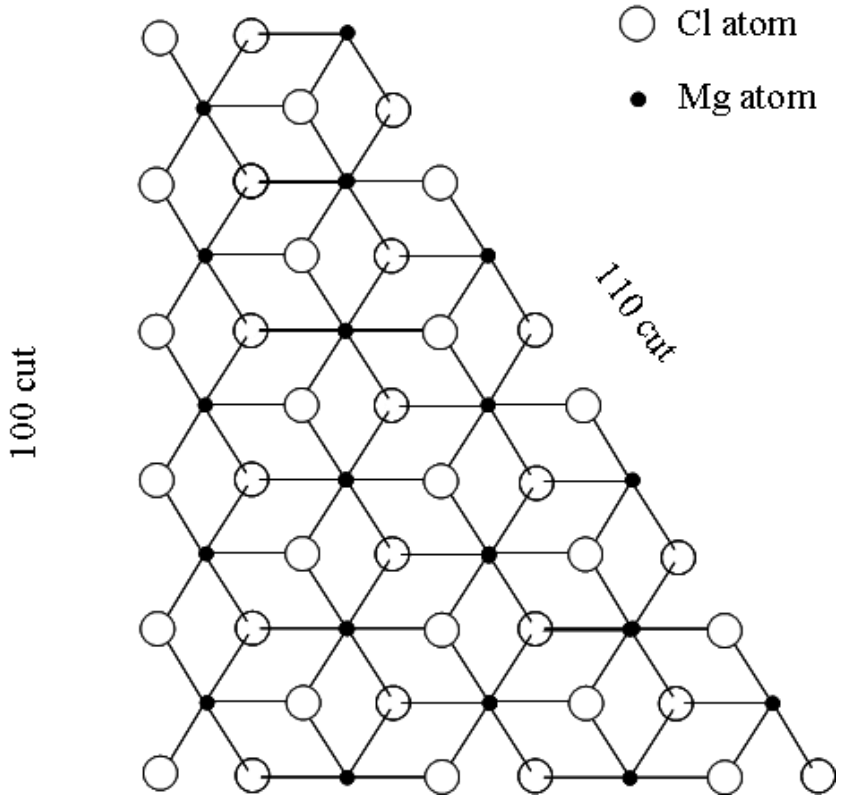

Figure 1.1. Model of $MgCl_2$ layer showing the (100) and (110) cuts

A fundamental question which arises in Ziegler-Natta catalysis is which crystallite face is most effective for coordination of the active site precursor, $TiCl_4$, and where the active species are located. In spite of numerous efforts, the exact nature of the various active species is still a subject of debate. For example, it has been suggested that dimeric species (Ti_2Cl_8) epitactically coordinated to the (100) lateral cut could lead to the formation of stereospecific active sites [5,6]. whereas recent

studies using FT-Raman spectroscopy have provided evidence for strong adsorption of $TiCl_4$ on the (110) lateral cut of $MgCl_2$, which gives a monomeric species with octahedrally coordinated titanium that can be the precursor for active and stereospecific sites [7,8].

After the discovery of high-activity $MgCl_2$-supported catalysts, it was soon realized that the internal donors and external donors must be used to improve their stereospecificity. Currently, as mentioned above, *mmmm* value of PP produced with the most widely used catalyst in which a phthalate and an alkoxysilane are used as the internal and external donors, respectively, reaches 97-99 wt.%. Donors strongly affect the catalytic properties such as the stereospecificity, the activity, the molecular weight distribution (MWD) of polymers, and the hydrogen response. The typical performance of combinations of internal donor and external donor is shown in Table 1.1 [9]. Even though a much efforts have been spent finding new donor systems to develop Ziegler-Natta catalyst system, precise understanding of the mechanism of the donors are still unclear. Busico et al. gave a explanation on the mechanism for donors to improve the isospecificity, donors have been considered to selectively adsorb on the (110) surface, resulting in an increase of the ratio of $TiCl_4$ dinuclear species on the (100) surface [10]. However, it has recently become more plausible that donors adsorb to the proximity of Ti species and act as a part of the active site [10-13].

Table 1.1. General performance of different electron-donor classes

Cat.	I.D.	E.D.	Yield (KgPP/gCat)	X.I. (%)	mmmm (%)	Mw/Mn	H_2 response
A	Phthalate	Silane	70-40	96-99	94-99	6.5-8	medium/low
B	Diether	Absent	130-100	96-98	95-97	5-5.5	excellent
B	Diether	Silane	100-70	98-99	97-99	4.5-5	excellent/high
C	Succinate	Silane	70-40	96-99	95-99	10-15	medium/low

I.D. = Internal Donor; E.D. = External Donor; X.I.= Xylene Insolubles; mmmm = isotactic pentads according to ^{13}C-NMR
The ranges are mainly function of the structure of I.D. and E.D. employed.
Bulk polymerisations at 70°C for 2 h, [$AlEt_3$] = 2.5 mM, Al/E.D. = 20 molar, [H_2] = as needed to obtain an intrinsic viscosity of 2 dl/g

1.3 Active sites of Ziegler-Natta Catalysts

Conventionally, the developments of the Ziegler-Natta catalysts have been done exhaustive and empirical method. Even this catalyst system have been widely applied in the industrial scene for more than 30 years (when the $TiCl_3$-$AlEt_2Cl$ system is included, it's over 50 years), the crucial factors governing the catalytic performance have not been amply clarified yet. To understand catalytic performance of each active site in Ziegler-Natta catalyst is vitally important to achieve desired polyolefin properties.

In the coordinative olefin polymerization field, a polymerization mechanism that proposed by

Cossee [14] have been assumed to be reliable, since it seems the best representation of what is happening at the active center (Figure 1.2). The titanium atom is in an octahedral coordination environment with one site vacant and an adjacent coordination site bonded to an alkyl group (polymer chain). For supported catalysts this structure is created when bound $TiCl_4$ reacts with aluminum alkyls such as $AlEt_3$

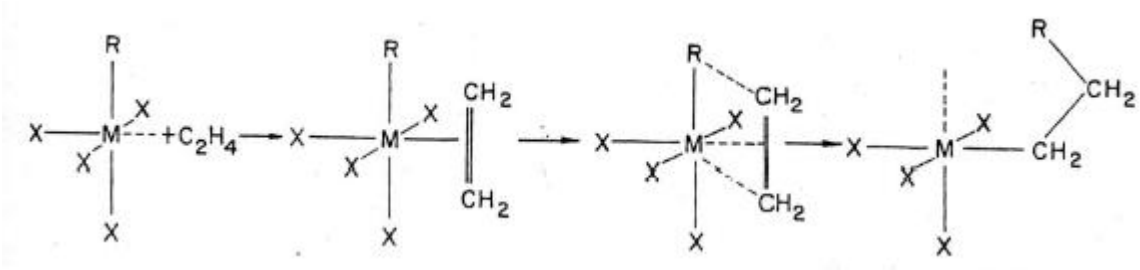

Figure 1.2. Cossee Mechanism. R and X indicate a growing chain and chlorine atom respectively.

Two-step mechanism for propagation involves p-coordination of an incoming monomer by the titanium atom at its vacant coordination site, followed by insertion, via a four-center transition state, into the titanium-alkyl (polymer) bond. It should be noted that for stereospecific polymerization, the growing polymer chain must migrate back to its original position after each insertion in order to maintain sterically identical propagation steps.

The insertion of an α-olefin in the metal-carbon bond may take place in two different ways:

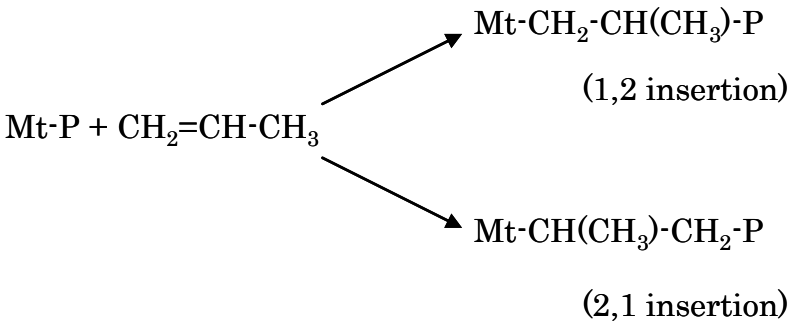

It is clearly proved, by chain-end group analysis, that the 1,2 insertion mode is working in isospecific polymerization of olefins with heterogeneous catalysts [15, 16].

Regioselectivity is extremely high in isotactic polymers obtained by heterogeneous catalysts [17]; head-to-head or tail-to-tail enchainments are sufficiently few as to be undetectable by IR and NMR spectroscopy. However, n-butyl end groups have been detected in propylene oligomers obtained with γ-$TiCl_3$/DEAC catalyst at high hydrogen concentration and in oligomers [18], and high molecular weight PP [19] prepared in the presence of hydrogen with $MgCl_2$/$TiCl_4$/dialkylphthalate-$AlEt_3$-alkoxysilane catalyst system. The proportion of isotactic polymer chains terminated by chain transfer with hydrogen after 2,1 insertion, leading to a *n*-butyl rather than to a *i*-propyl group, according to the following scheme,

$$Ti\text{-}CH(CH_3)\text{-}CH_2\text{-}CH_2\text{-}CH(CH_3)\text{-}P + H_2 \longrightarrow Ti\text{-}H + CH_3\text{-}(CH_2)_3\text{-}CH(CH_3)\text{-}P$$

$$Ti\text{-}CH_2\text{-}CH(CH_3)\text{-}CH_2\text{-}CH(CH_3)\text{-}P + H_2 \longrightarrow Ti\text{-}H + CH_3\text{-}CH(CH_3)\text{-}CH_2\text{-}CH(CH_3)\text{-}P$$

is 12 to 28 %, depending on the kind of alkoxysilane used. We can conclude, therefore, that an occasional 2,1 insertion is possible at isotactic centers in heterogeneous catalyst but this irregular placement precludes any further monomer insertion.

Considering that α-olefin are prochiral, that is, they have two different sides (the two R,S enantiofaces are shown in Figure 1.3), the absolute configuration of the tertiary carbon atoms of the main chain (R) or (S) is dictated by the enantioface undergoing the insertion, the insertion mode, and the stereochemistry (cis or trans) of the insertion [20].

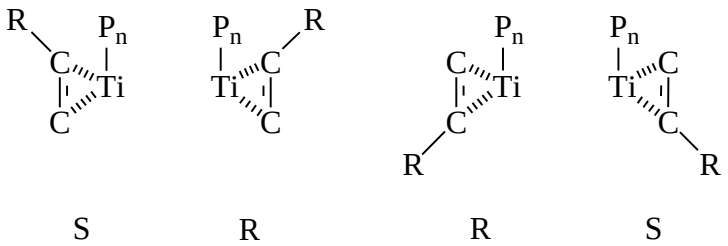

Figure 1.3. The different enantiofaces of the olefin and their ossible coordination mode to the

active center.

If regioselectivity is high and insertion occurs only with cis stereochemistry, multiple insertions of the same enantioface produce a polymer chain with chiral centers of the same configuration (i.e., an isotactic polymer); multiple insertions of alternating enantiofaces produce a polymer chain with chiral centers alternating configuration (i.e., a syndiotactic polymer); random enantioface insertion produce a polymer chain with no configuration regurality (i.e., an atactic polymer).

To discriminate between two prochiral faces of the olefin, the catalyst system must possess at least one chirality center. A chiral carbon atom is present in the growing chain in beta or alpha position with respect to the metal atom, depending on the 1,2 or respectively 2,1 insertion mode. The mechanism of stereochemistry determined by chiral induction by the last unit is referred to as chain end control. A second possible element of chirality is the asymmetry of the initiating site; in this case, the stereoselection mechanism is referred to as enantiomorphic site control (Figure 1.4).

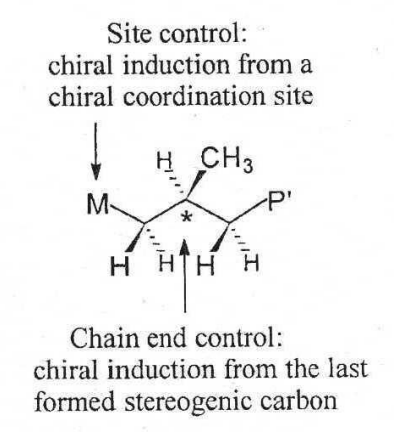

Figure 1.4. The two possible sources of enantioface selectivity.

Steric errors during the chain growth lead to different chain microstructures which are therefore diagnostic of the stereoselection mechanism (Figure 1.5).

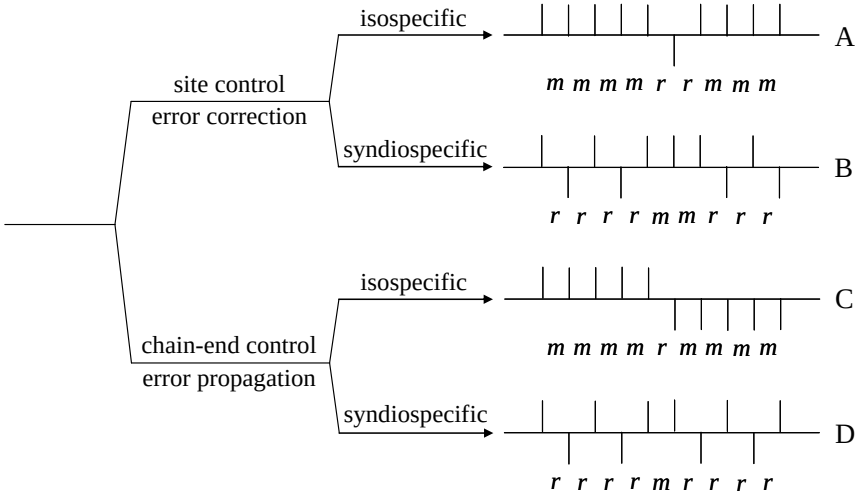

Figure 1.5. The four possible stereospecific mechanisms leading to ordered polymer structures. A chain segment with the diagnostic isolated insertion of mistake is shown in ites modified Fisher

projection for each case.

The following experimental data are consistent with an enantiomorphic site control of the reaction in the isospecific polymerization of α-olefins.

1. Stereoirregularities in isotactic polymers consist of pairs of syndiotactic racemic (r) dyads connecting stereosequences of isotactic meso (m) dyads of the type mmmrrmmm, corresponding to the idealized structure A of Figure 1.5; that is, the formation of a configuration error does not affect the configuration of the following monomer unit [21].
2. The retention of the configuration in the growing chain is preserved after the insertion of an ethylene unit [22].
3. Isospecific catalytic sites show stereoselectivity in racemic α-olefins polymerization [23].
4. A straightforward evidence against chain end stereochemical control in isospecific polymerization is given by end-groups ^{13}C NMR analysis of isotactic polybutene obtained with $TiCl_3/AlEt_3$ enriched with ^{13}C at the methylene carbons. The end groups resulting from insertion of two monomer unites into a Ti-$^{13}CH_2$-CH_3 bond are stereoregular, despite the absence of asymmetry in the original ethyl group and in the alkyl group resulting after the first

insertion [15, 24].

$TiCl_3$ Catalyst Models

A great number of models for catalytic centers have been proposed to interpret the isospecific polymerization of olefins with Ziegler-Natta catalysts.

Arlman and Cossee proposed that the active sites in γ-$TiCl_3$ are located on lateral crystal surfaces which corresponds to (110) planes [25]. Titanium atoms present on the planes have a vacant octahedral site and are bonded to five chlorine atoms. One chloride ligand protrudes from the surface, the other four are bridged to further Ti atoms and are more strongly bound; neighboring Ti atoms have opposite chilarity [26,27]. By reaction with the cocatalyst, the single bonded Cl atom should be easily substituted by an alkyl group, giving the active Ti-C bond.

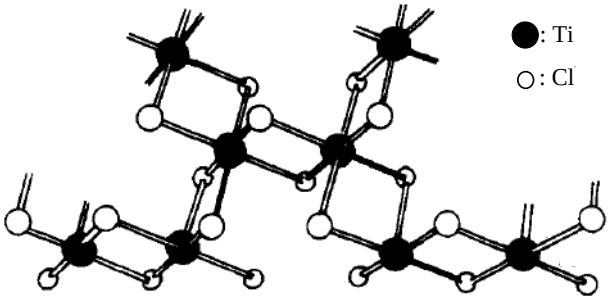

Figure 1.6. Schematic drawing of a lateral cut of a $TiCl_3$ layer. The chirality of two titanium

atoms is indicated.

The surface model proposed by Allegra obviates the necessity of the back skip step to assure the stereoselectivity because a C_2 symmetry axis locally relates the atoms relevant to the non-bonded interactions with the monomer and the growing chain [28]. Therefore, the two situations resulting by exchanging in the coordination step, the relative positions of the growing chain and of the incoming monomer are identical.

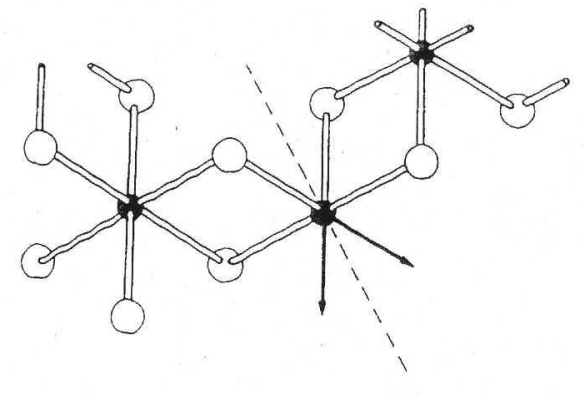

Figure 1.7. The $TiCl_3$ layer termination proposed by Allegra; the arrows indicate the two equivalent coordination positions related by a two fold axis.

Corradini et al. suggest that the chiral environment of the metal atom imposes a chiral orientation

of the first C-C bond of the chain, and this orientation has been identified as a crucial factor in determining the stereospecificity. They evaluated non-bonding interaction by calculation, which will be discussed later. Three sites model of active sites in $TiCl_3$ was proposed [29].

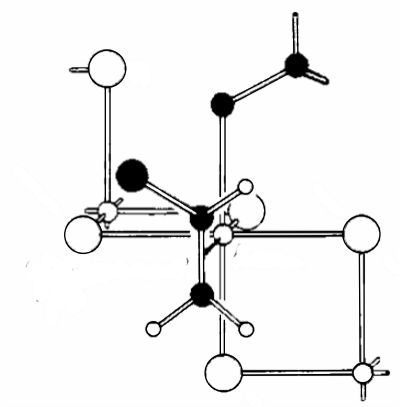

Figure 1.8. Schematic drawing of the local environment of a catalytic site located at a relief of the lateral surface of $TiCl_3$

$MgCl_2$-Supported Catalyst Models

Busico et al. showed that reduced $TiCl_4$ on the (1 0 0) $MgCl_2$ crystal face has two vacancies and the (1 1 0) face has only one [30,31]. Dimerized $TiCl_3$ on the (100) face are believed to be stereospecific sites since they are in a chiral environment.

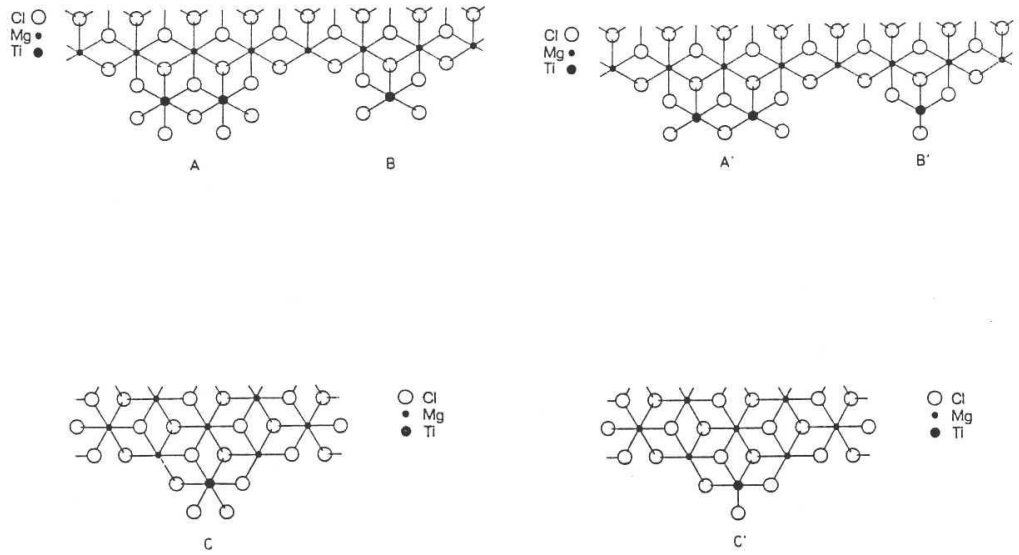

Figure 1.9. Possible models of Ti(IV) complexes coordinated to the (100) faces (A and B), (110) faces (C) of $MgCl_2$; the same after activation by Al-Alkyl (catalytic sites A', B' and C', respectively). The position of non-bridge chlorine atoms is only indicative.

Vacant sites are necessary for polymerization, but sites with more than one vacancy are aspecific, as shown Sun and Soga [32]. Then, Soga et al. and Kuroda et al. proposed site poisoning mechanism as shown in Figure 1.10 [33, 34].

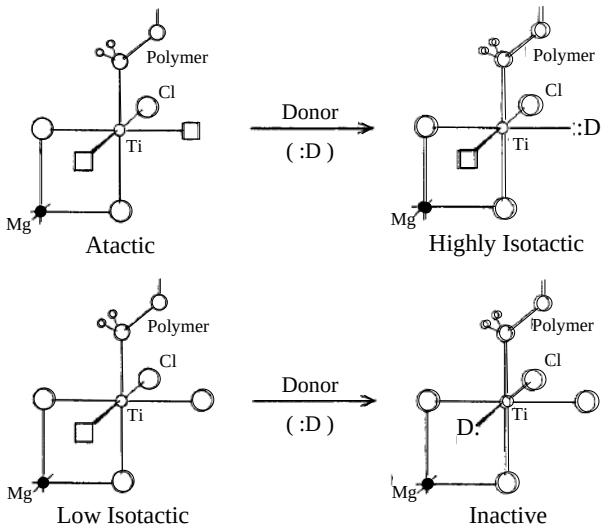

Figure 1.10. Models for the active sites on $MgCl_2$ supported Ti catalyst and the effect of an electron donor

Based on ^{13}C NMR data, Doi et al. [35] proposed an active site model where there is a strictly stereospecific site and a second site which can be converted between stereospecific and aspecific by reversible $AlEt_3$ migration as shown in Figure 1.11.

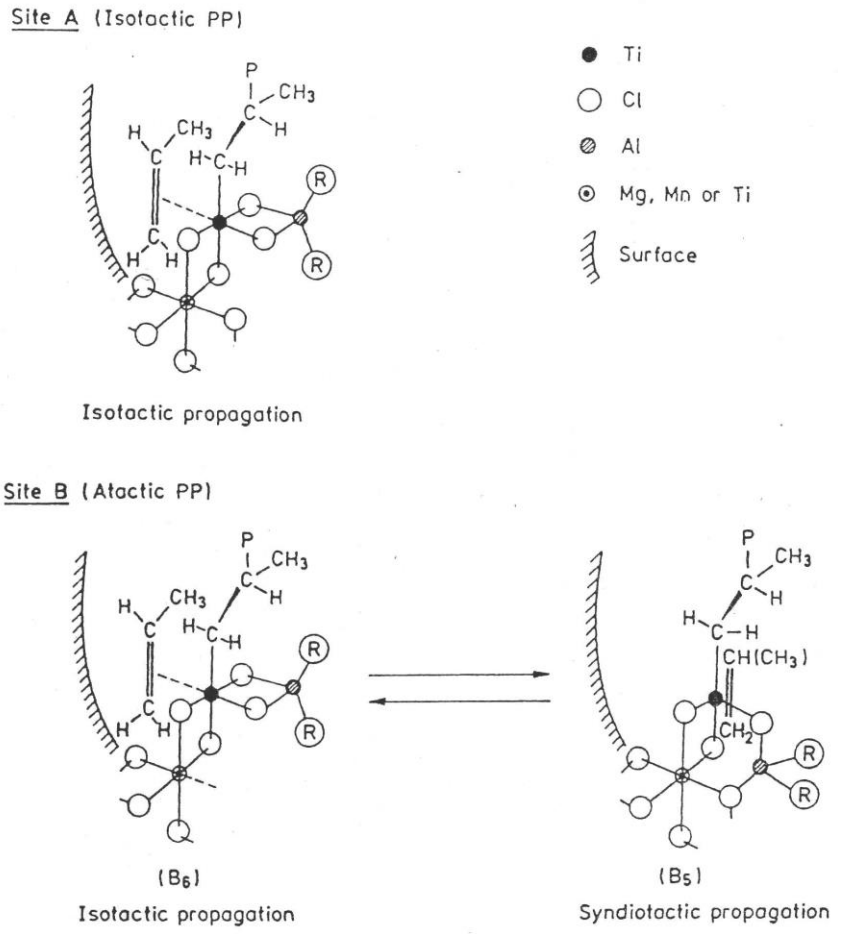

Figure 1.11. Model of bimetallic active site proposed by Doi et al

Recently, Corradini and Busico et al. proposed a three-sites model [36] on the basis of the stereosequence distribution of the atactic and isotactic fractions of PP obtained with a $MgCl_2$-supported catalyst determined by high-resolution ^{13}C NMR analysis [37-40]. These fractions comprise the same three building blocks (highly isotactic, weakly isotactic, and

syndiotactic sequences) and differ only in their relative amounts. The stereoblock nature implies the presence of three sites, namely, highly isospecific site, weakly isotactic (isotactoid) site, and syndiospecific site, and reversible switches between them. They suggested that these switches are caused by ligand exchanges at position L1 and L2 in Figure 1.12.

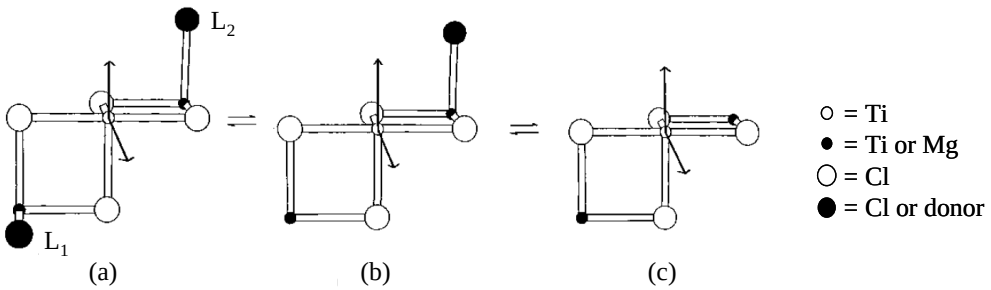

Figure 1.12 Possible models of active species for (a) highly isotactic, (b) isotactoid, (c) syndiotactic propagation.

Terano et al. proposed the further modification of three-sites model based on the detailed analysis of PPs obtained with a donor-free $MgCl_2/TiCl_4$ catalyst [41].

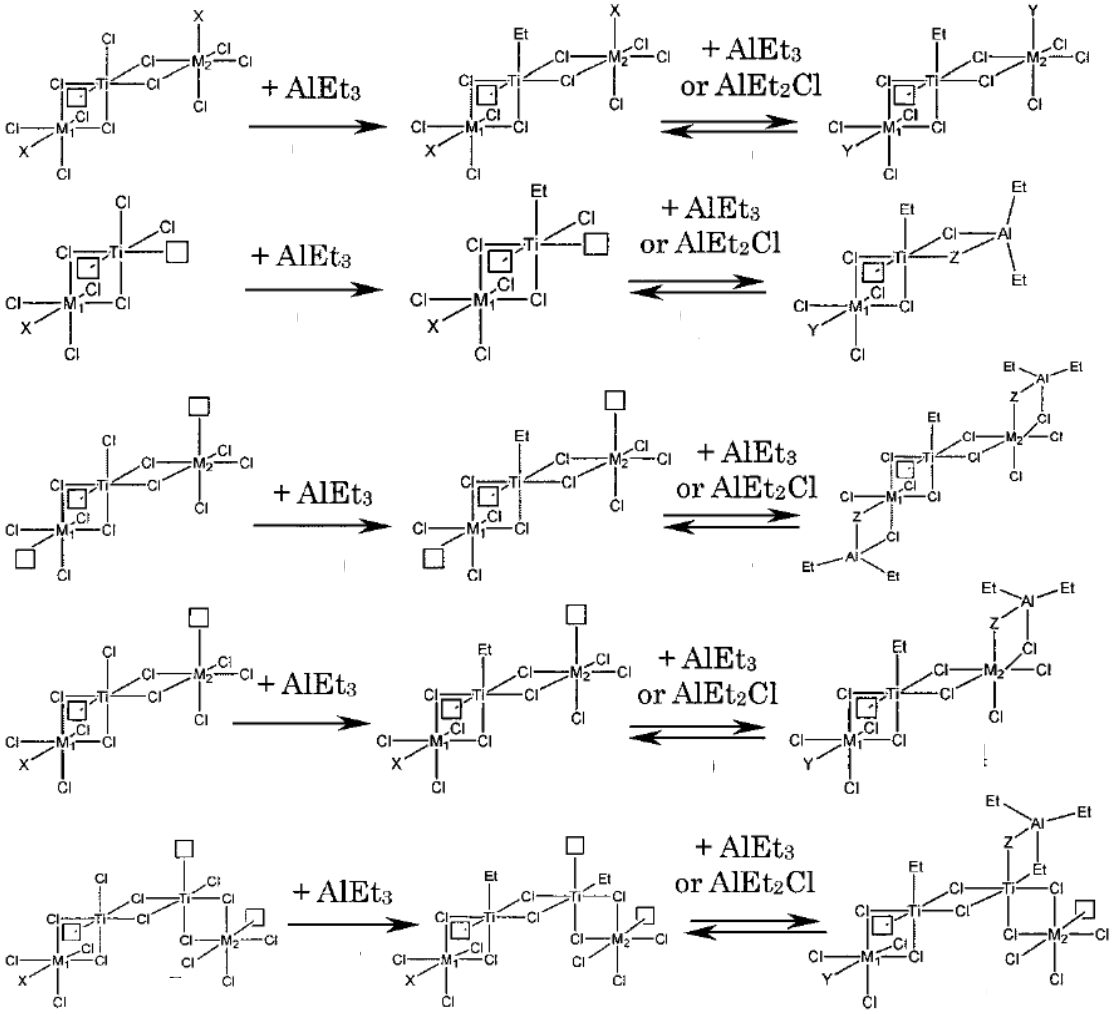

Figure 1.13. Modified three-sites model proposed by Terano et al.

1.4 Model Catalysts for $MgCl_2$-Supported Ziegler-Natta Catalysts

For understanding this complex catalyst system, it is supposed to be effective to apply model catalyst. A much effort has been paid in this subject. Some of them will be introduced in this section.

Busico et al. reported homogeneous C_2-Symmetric Octahedral Zr(IV) Complexes for Ziegler-Natta model[42]. They concluded that, as far as the regio- and enantioselectivity of propylene insertion and the processes of chain transfer are concerned, the two investigated catalysts are good models of Ziegler-Natta active species. On the other hand, compared with the latter, the absolute rates of chain propagation and transfer are much lower.

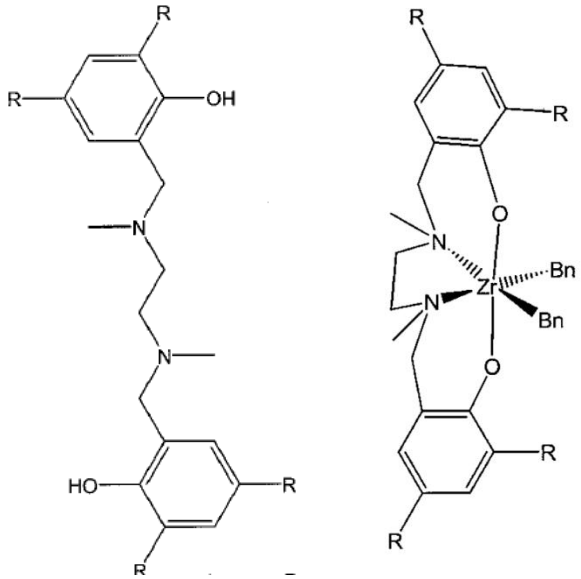

Figure 1.14. Schematic drawing of the two tetradentate [ONNO] ligands, and of the

corresponding Zr(IV) complexes.

Groppo et al. investigated the structural, vibrational, and optical properties of Ti and Mg chloride tetrahydrofuranates as precursors of heterogeneous Ziegler–Natta catalysts by X-ray powder diffraction(XRPD), Infrared, Raman, and UV/Vis spectroscopy[43]. Those presented are among the first direct experimental data on the structure of the active Ti sites in Ziegler–Natta catalysts, and can be used to validate the many computational studies that have been increasing exponentially in the last few decades.

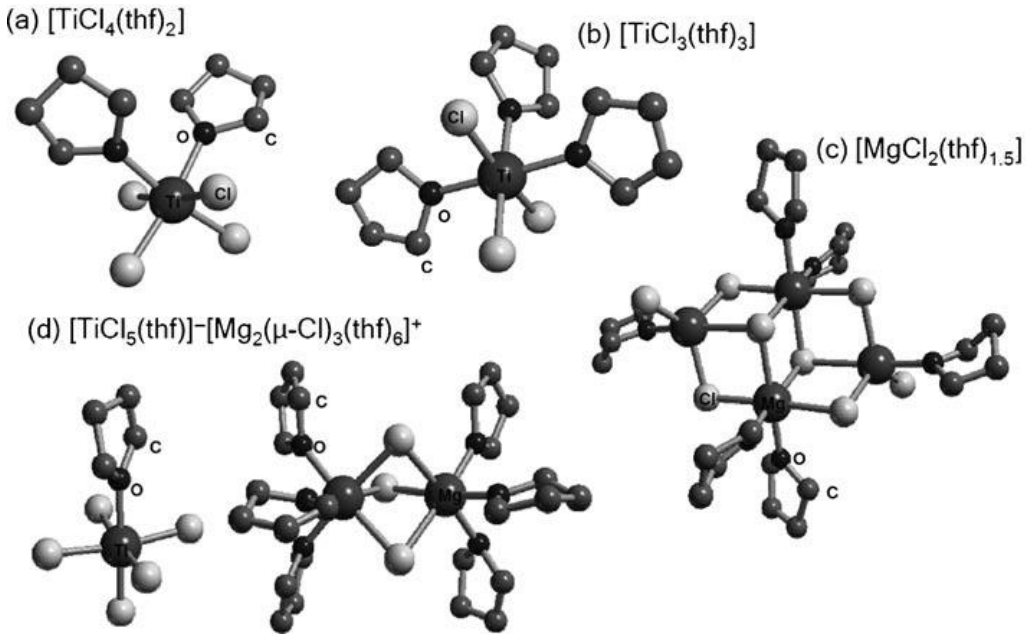

Figure 1.15. Molecular units constituting the crystal structures of the three tetrahydrofuranate

precursors of Ziegler–Natta catalysts and of the bimetallic salt.

Terano et al. reported relationship between Ti dispersion state and propylene polymerization properties with $MgCl_2$-supported $TiCl_3$ model catalyst prepared using $TiCl_3$·3Pyridine complex [44]. This model catalyst can control the dispersion state of Ti species by changing the Ti content, and can reduce active sites heterogeneity. However produced PPs still exhibited polydispersity.

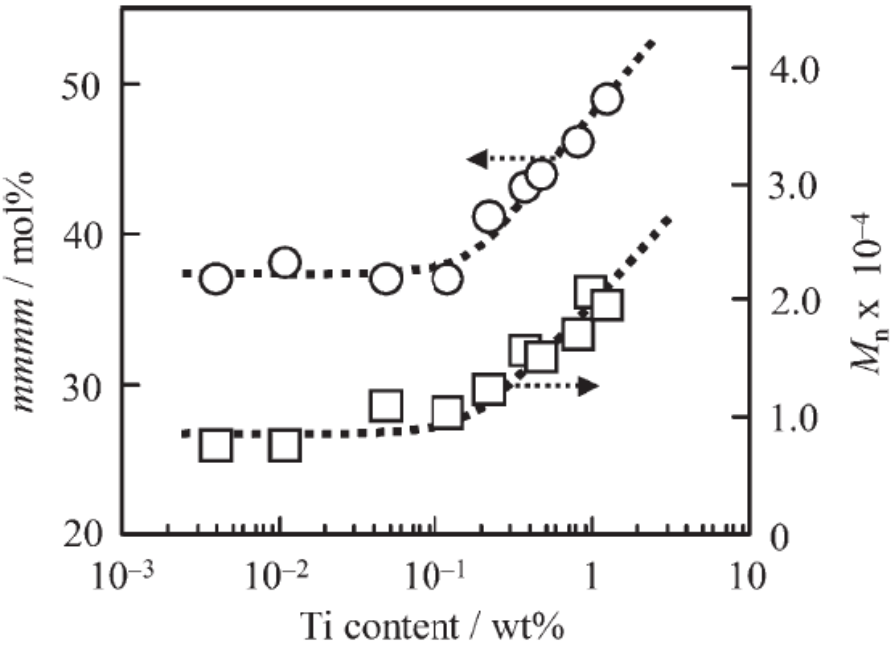

Figure 1.16. Stereoregularity (○) and M*n* (□) of the PPs vs. Ti content

They also investigated to develop core–shell $MgO/MgCl_2/TiCl_4$ model catalysts [45]. The MgO

nanoparticles were utilized as a non-fragmentable core material to prepare novel core‑shell $MgO/MgCl_2/TiCl_4$ catalysts for olefin polymerization. With these model catalysts, structure–performance relationship between the catalyst surface area and propylene polymerization activity was successfully obtained.

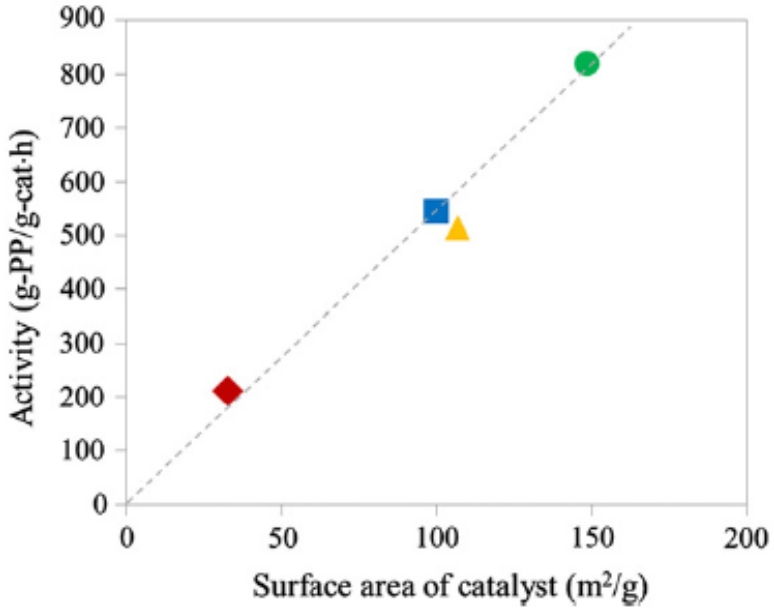

Figure 1.16. Relationship between the catalyst surface area and propylene polymerization activity.

Andoni et al. reported new surface science model for Ziegler-Natta catalyst [46,47]. In that reports, a method for the preparation of well-defined crystallites of $MgCl_2$-supported Ziegler-Natta

catalysts on Si wafers has been developed. The growth of the crystallites on the flat silica facilitates their characterization using electron and scanning probe microscopy. The relative proportions of 120º and 90º edge angles indicate the preference for the formation of a particular crystallite face for the $MgCl_2$ (Figure 1.17).

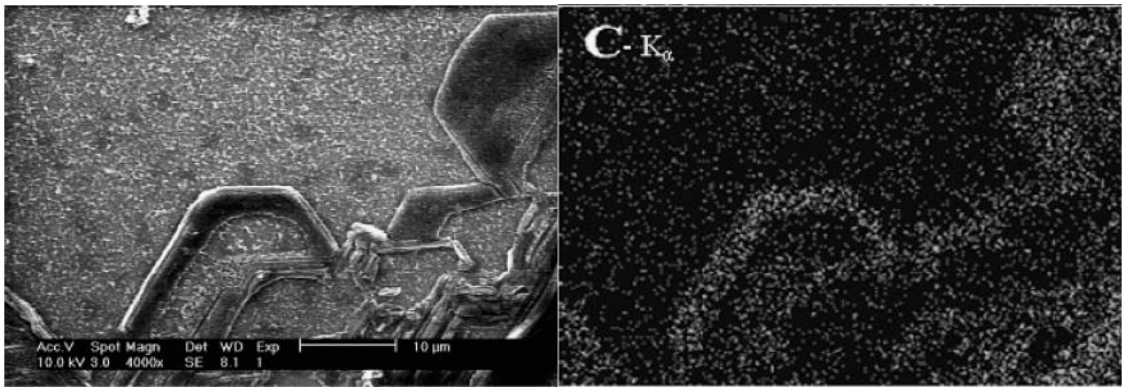

Figure 1.17. SEM image (left) and SEM-EDX mapping of C Ka (right) of polyethylene obtained after 3 min polymerization on silica wafer. The polymer growth at the edges of the crystallites clearly indicates the presence of the active site precursor, $TiCl_4$ or $TiCl_n(OEt)_4 \cdot n$.

1.6 Objective of This Study

Polyolefin such as polypropylene and polyethylene produced with Ziegler-Natta catalysts is one of the largest markets. Research about the nature of Ziegler-Natta catalysts is ongoing because of the industrial importance for development of new grades of PP. However, despite extensive efforts, there is still limited understanding of the nature of Ziegler-Natta catalysts, especially this is because the nature of active sites. Molecular-level understanding of surface events, a prerequisite for tailor-made design of heterogeneous catalysis, is usually highly challenging for powder catalysts because their surfaces are (more or less) chemically and structurally heterogeneous as well as dynamic. The heterogeneity has inhibited the direct characterization of active sites, the evaluation of the catalytic performance of each active site, and the understanding of molecular-level behaviors of the catalysts. One of the helpful ways to address problems of the multisite nature is to employ using model catalysts which can reduce heterogeneity.

The object of this dissertation is to develop novel Ziegler-Natta model catalysts which are useful to clarify active site natures. In Chapter 2, single-site Ti-based polymerization catalysts such as titanocenes were immobilized on $MgCl_2$ to develop single-site Ziegler-Natta model catalysts. The single-site nature of these complexes enables to suppress the formation of Ti clusters by bulky

ligands, to change steric and electronic environments of the Ti center by using various ligands and to clarify effects of immobilization on $MgCl_2$. In Chapter 3, a realistic synthetic route for the active $MgCl_2$ surfaces has discovered by donor-induced reconstruction under UHV conditions. Finally, general conclusion is described in chapter 4.

Reference

[1] 次世代ポリオレフィン総合研究会編, *次世代ポリオレフィン総合研究*, **2012**, Vol. 6

[2] E. Albizzati, U. Giannini, G. Collina, L. Noristi, L. Resconi, "*Propylene Handbook,*", E. P. Moore, Ed., Hanser, New York, **1996**, Chapter 2.

[3] G. Giunchi, G. Allegra, *J. Appl. Cryst*, **1984**, *17*, 172.

[4] U. Giannini, Makromol, *Chem. Suppl*, **1981**, *5*, 216.

[5] P. Corradini, V. Busico, G. Guerra, "*Transition Metals and Organometallics as Catalysts for Olefin Polymerization*", W. Kaminsky, H. Sinn, Eds., Springer, Berlin, **1988**, 337.

[6] V. Busico, P. Corradini, L. De Martino, A. Proto, V. Savino, E. Albizzati, *Makromol. Chem*, **1985**, *186*, 1279.

[7] L. Brambilla, G. Zerbi, S. Nascetti, F. Piemontesi, G. Morini, *Macromol. Symp*, **2004**, *213*, 287.

[8] L. Brambilla, G. Zerbi, F. Piemontesi, S. Nascetti, G. Morini, *J. Mol. Catal., A: Chem.*, **2007**, *263*, 103.

[9] G. Cecchin, G. Morini, A. Pelliconi, *Macromol. Symp.*, **2001**, *173*, 195.

[10] M. C. Sacchi, I. Tritto, P. Locatelli, *Prog. Polym. Sci.*, **1991**, *16*, 331.

[11] J. C.Chadwick, G. Morini, G. Balbontin, I. Camurati, J. J. R. Heere, I. Mingozzi, F. Testoni, *Macromol. Chem. Phys.*, **2001**, *202*, 1995.

[12] J. C. Chadwick, *Macromol. Symp.*, **2001**, *173*, 21.

[13] T. Taniike, M. Terano, *Macromol. Rapid Commun.*, **2007**, *28*, 1918.

[14] P. Cossee, *J. Catal.*, **1964**, *3*, 80.

[15] A. Zambelli, P. Locatelli, M.C. Sacchi, I. TrittoA. Zambelli, P. Locatelli, M.C. Sacchi, I. Tritto, *Macromolecules*, **1982**, *15*, 831.

[16] M.C. Sacchi, I. Tritto, P. Locatelli, *Prog. Polym. Sci.*, **1991**, *16*, 331.

[17] C. Wolfsgruber, G. Zannoni, E. Rigamonti, A. Zambelli, *Makromol. Chem.*, **1975**, *176*, 2765.

[18] V. Busico, P. Cipullo, P. Corradini, *Makromol. Chem., Rapid Commun.*, **1992**, *13*, 15.

[19] J.C. Chadwick, A. Miedema, O. Sudmeijer, *Makromol. Chem.*, **1994**, *195*, 167.

[20] P. Pino, R. Mulhaupt, *Angew. Chem. Int. Ed. Engl.*, **1980**, *19*, 857.

[21] Y. Doi, T. Asakuru,, *Makromol. Chem.*, **1975**, *176*, 507.

[22] W.O.Jr. Crain, A. Zambelli, J.D. Roberts, *Macromolecules*, **1971**, *4*, 330.

[23] P. Pino, *Adv. Polym. Sci.*, **1965**, *4*, 393.

[24] P. Locatelli, I. Tritto, M.C. Sacchi, *Makromol. Chem., Rapid Commun*, **1984**, *5*, 465.

[25] E.J. Arlman and P. Cossee, *J. Catal.*, **1964**, *3*, 99.

[26] P. Corradini, G. Guerra, *Prog. Polym. Sci.*, **1991**, *16*, 239.

[27] P. Corradini, V. Busico, G. Guerra, "*Comprehensive Polymer Science*", G.C. Eastmann, A. Ledwith, S. Russo, P. Sigwalt, Eds., Pergmon Press, **1989**, *4*, 2950.

[28] G. Allegra, *Makromol. Chem.*, **1971**, *145*, 235.

[29] P. Corradini, V. Barone, B. Fasco, G. Guerra, *J. Catal.*, **1982**, *77*, 32.

[30] V. Busico, P. Corradini, D. Martino, A. Proto, V. Savino, E. Albizzati, *Makromol. Chem.*, **1986**, *187*, 1115.

[31] V. Busico, P. Corradini, A. Ferraro, A. Proto, V. Savino, E. Albizzati, *Makromol. Chem.*, **1986**, *187*, 1125.

[32] L. Sun and K. Soga, *Makromol. Chem.*, **1989**, *190 (12)*, 3137.

[33] K. Soga, T. Shiono, Y. Doi, *Polym. Bull.*, **1983**, *10*, 168.

[34] N. Kuroda, Y. Nishikitani, K. Matsuura, M. Miyoshi, *Makromol. Chem.*, **1987**, *188*, 1897.

[35] Y. Doi, *Makromol. Chem., Rapid Commun.*, **1982**, *3*, 635.

[36] V. Busico, R. Cipullo, G. Monaco, G. Talarico, M. Vacatello, J.C. Chadwick, A.L. Segre, O. Sudmeijer, *Macromolecules*, **1999**, *32*, 4173.

[37] V. Busico, P. Corradini, R.D. Biasio, L. Landriani, A.L. Segre, *Macromolecules*, **1994**, *27*, 4521.

[38] V. Busico, R. Cipullo, P. Corradini, L. Landriani, M. Vacatello, A.L. Segre, *Macromolecules*, **1995**, *28*, 1887.

[39] V. Busico, R. Cipullo, G. Monaco, M. Vacatello, A.L. Segre, *Macromolecules*, **1997**, *30*, 6251.

[40] V. Busico, R. Cipullo, G. Monaco, M. Vacatello, J. Bella, A.L. Segre, *Macromolecules*, **1998**, *31*, 8713.

[41] L. Boping, T. Nitta, H. Nakatani, M. Terano, Macromol., *Chem. Phys.*, **2002**, *203*, 2412.

[42] V. Busico, R. Cipullo, S. Ronca, P. H. M. Budzelaar, *Macromol.Rapid Commun.* **2001**, *22*, 1405.

[43] K. Seenivasan, A. Sommazzi, F. Bonino, S. Bordiga, E. Groppo, *Chem. Eur. j.* **2011**, 17, 8648.

[44] T. Wada, T. Taniike, I. Kouzai, S. Takahashi, M. Terano, *Macromol.Rapid Commun.* **2009**, *30*, 887.

[45] T. Taniike, P. Chammingkwan, M. Terano, *Catal. Commun.* **2012**, *27*, 13.

[46] A. Andoni, J. C. Chadwick, H. J. W. Niemantsverdriet, P. C. Thune, *Macromol. Rapid. Commun.*, **2007**, *28*, 1466.

[47] A. Andoni, J. C. Chadwick, H. J. W. Niemantsverdriet, P. C. Thune, *J. Catal.*, **2007**, *247*, 129.

Chapter 2

Control of Active Site Structure and Propylene Polymerization Properties of $MgCl_2$-Supported Titanocene Catalysts

2.1 Introduction

In the production of isotactic polypropylene, the design of active site structure is one of the major targets for the development of new catalysts, since they dominate stereoregularity, molecular weight, and chemical composition of resulting polymer. Though both heterogeneous Ziegler-Natta catalysts and homogeneous organometallic complexes (especially IV group metallocene catalysts) have an ability to produce polypropylene which can be classified as isotactic polypropylene, the resulting polymer structures are largely different between the two catalysts due to the different active site natures. Ziegler-Natta catalysts produce polydisperse isotactic polypropylene with concentrated stereoerrors and high regioregularity, generally resulting in a higher melting point.[1] On the other hand, typical ansa-metallocene catalysts produce monodisperse polypropylene with stereoerrors randomly distributed over the backbone as well as lower regioregularity.[2]

Industrial heterogeneous Ziegler-Natta catalysts consist of $TiCl_4$ supported on $MgCl_2$ combined with Lewis base compounds (called as donors) and trialkylaluminum. Their active species are regarded as neutral Ti(III)-alkyl species, situated in a pseudo octahedral symmetry. It is well accepted within a three site model that the isospecificity is originated from ligands coordinated at metal ions adjacent to an active Ti center.[3,4] Further details on the active sites such as the

placement of $TiCl_4$ on $MgCl_2$ surfaces and the identity of stereo-regulating ligands are still ambiguous, mainly due to difficulties in the characterization of active sites and the polydispersity itself in polymer structures. Consequently, the structures of isotactic polypropylene have been empirically controlled in its industrial production, based on different combinations of internal and external donors.

Active species of C_2 metallocene catalysts of group IV metals are cationic M(IV)-alkyl with a pseudo tetrahedral symmetry, where the isospecificity results from bulky bis-cyclopentadienyl derivatives.[5,6] Since metallocene complexes exhibit a single-site nature, a clear relationship between the structures of the active site and resultant polymer has been established.

On the other hand, commercialization of metallocene catalysts necessarily requires their immobilization onto a suitable support from a viewpoint of morphology control of produced polymer. A variety of immobilization techniques have been developed, which can be roughly classified into i) direct impregnation of complexes on supports mostly pre-treated with alkylaluminum,[7,8] ii) impregnation of activators such as methylaluminoxane (MAO) (called as supported activators),[9,10] and iii) tethering complexes on support surfaces through covalent link between supports and ancillary ligand frameworks.[11-14] A key issue in the immobilization is to

suppress unfavorable interaction and reaction between complexes and supports and to keep their original active site natures, where SiO_2 is the most widely studied support.

In contrast, several researchers have attempted to facilitate strong interaction between complexes and $MgCl_2$ support for improved catalyst performances, as is the case for heterogeneous Ziegler-Natta catalysts, where the immobilization of $TiCl_4$ on $MgCl_2$ results in progressive enlargements in the propagation rate constant and the number of active sites.[15-18]

The majority of these researches studied ethylene (co)polymerization while only a few reported for propylene polymerization.[19-30] For example, Sivaram et al. reported that active species derived from titanocene dichloride were stabilized by $MgCl_2$ during ethylene polymerization.[19] Soga et al. reported that a zirconocene catalyst supported on $MgCl_2$ pre-treated with alkylaluminum was activatable with alkylaluminum, and gave polydisperse polypropylene.[20] The same authors found that the addition of external donor improved the stereoregularity of isotactic polypropylene produced by $MgCl_2$-supported half-titanocene.[21] Ishihara et al. also reported that half-titanocene catalysts ground with $MgCl_2$ in the presence of alkylaluminum and borate produced isotactic polypropylene, unlike the homogeneous catalysts.[22] On the other hand, titanocene complexes impregnated on $MgCl_2/AlR_m(OEt)_{3-m}$ supports kept the single-site nature of the

complexes in ethylene polymerization, while the supported complexes were activatable only with alkylaluminum.[23,24] Thus, metallocene catalysts supported on $MgCl_2$ have exhibited catalytic aspects quite similar to those of heterogeneous Ziegler-Natta catalysts. However, the active site natures of $MgCl_2$-supported metallocene catalysts have not been systematically and sufficiently examined in comparison with those of Ziegler-Natta catalysts to explore for model system of traditional Ziegler-Natta catalysts. Furthermore, it is significant in developing synergized supported metallocene catalysts to examine effects of variables such as the immobilization method as well as the kinds of metallocene complexes and activators on the active site natures.

In this study, various $MgCl_2$-supported Cp_2TiCl_2, $CpTiCl_3$ and $TiCl_4$ catalysts were synthesized based on different immobilization procedures, and the resultant active site natures in propylene polymerization using alkylaluminum or MAO were systematically compared to find a possibility of synergetic metallocene-support interaction. According to the immobilization procedure and the kind of activators, two classes of active sites were formed: active sites typical for Ziegler-Natta catalysts to produce isotactic polypropylene, whose stereoregularity was improved by the addition of external donors, and those typical for titanocene catalysts to produce rather atactic polypropylene, whose activities were greatly enhanced by using polar solvents as polymerization medium. This

diversity of the active site natures plausibly originated from the oxidation state of supported titanocene during polymerization.

2.2 Experimental Section

2.2.1 Materials

Propylene of research grade was used without further purification. Toluene and dichloromethane (purchased from Kanto Chemical Co., Inc.) for polymerization solvent were dried by passing through a column with the molecular sieve 4A. Toluene for catalyst preparation was purified by refluxing over sodium followed by distillation. Modified methylaluminoxane (MMAO-3A) and triethylaluminum (TEA) were donated by Tosoh Finechem Co. Cyclohexylmethyldimethoxysilane (CMDMS, purchased from Sigma-Aldrich Co. LLC) was purified by distillation. Anhydrous magnesium dichloride with a specific surface area of 65.1 $m^2 \cdot g^{-1}$ ($MgCl_2$, donated by Toho Titanium Co., Ltd.), bis(cyclopentadienyl)titanium dichloride (Cp_2TiCl_2) and cyclopentadienyl titanium trichloride ($CpTiCl_3$, both purchased from Gelest, Inc.), and titanium tetrachloride ($TiCl_4$, purchased from Wako Pure Chemical Industries, Ltd.) were used as delivered.

2.2.2 Catalyst preparation

Supported catalysts were prepared based on the following two methods.

Physical method: $MgCl_2$ (4.0 g) was ground with toluene (30 mL) solution containing Cp_xTiCl_{4-x} (x = 2 or 1) or $TiCl_4$ (0.3 mmol) at room temperature using rotary ball mill for 40 h under nitrogen atmosphere. The synthesized catalysts were designated as $Cp_2TiCl_2/MgCl_2$(P), $CpTiCl_3/MgCl_2$(P), and $TiCl_4/MgCl_2$(P).

Chemical method[20]: $MgCl_2$ 10.4 g and 1.18 mmol of Cp_xTiCl_{4-x} (x = 2-0) or $LTiCL_3$ (L = Pentamethylcyclopentadienyl, Indenyl)were contacted in the presence of 42 mmol of TEA in 371 mL of toluene at room temperature for 10 min (named as $Cp_2TiCl_2/MgCl_2$(C), $CpTiCl_3/MgCl_2$(C), $TiCl_4/MgCl_2$(C), $IndTiCl_3/MgCl_2$(C), $Cp^*TiCl_3/MgCl_2$(C)).

All supported catalysts were repeatedly washed with distillated toluene until unsupported complexes in supernatant liquid were not detected by UV-vis spectroscopy (JASCO V-670). The Ti contents were measured after dissolving catalysts in aqueous H_2SO_4/HCl/H_2O_2 by UV-vis spectroscopy (Table 1).

Table 1. Titanium content of the catalysts

Catalyst	Ti content (wt.%)
$Cp_2TiCl_2/MgCl_2$(P)	0.085
$CpTiCl_3/MgCl_2$(P)	0.076
$TiCl_4/MgCl_2$(P)	0.64
$Cp_2TiCl_2/MgCl_2$(C)	0.067
$CpTiCl_3/MgCl_2$(C)	0.28
$TiCl_4/MgCl_2$(C)	0.54

2.2.3 Polymerization

Propylene polymerization was conducted in a 1 L stainless steel reactor equipped with an agitating blade. Toluene or dichloromethane (200 mL) was introduced into the reactor under nitrogen atmosphere and then propylene gas was saturated at 5 atm for 30 min. After propylene saturation, activator (4.0 mmol of MMAO or 2.0 mmol of TEA) was introduced into the reactor. To start the polymerization, a measured amount of a catalyst was added to make the Al/Ti molar ratio 500 $mol \cdot mol^{-1}$. Propylene was continuously supplied to keep constant pressure during

polymerization. Polymerization was terminated after 30 min by adding ethanol. For reference, polymerization with unsupported Cp_2TiCl_2 and $CpTiCl_3$ complexes was conducted under the completely same conditions. In polymerization with donor (CMDMS), donor (Al/donor = 20 for MMAO and 10 for TEA mol·mol^{-1}) was added to the reactor after injection of activator, followed by the catalyst slurry injection to start the polymerization. Obtained polymer was then washed with distilled water three times and dried in vacuo at 60ºC for 6 h. Thereafter, polymer was dissolved in xylene containing 0.03 wt.% 2,6-*t*-butyl-4-methylphenol and precipitated by an excess amount of cold acetone. The polymer was finally filtered and dried in vacuo at 60ºC for 6 h.

2.2.4 Polymer characterization

The molecular weight (M_n) and molecular weight distribution (M_w/M_n) of polypropylene was measured by gel permeation chromatography (Waters Associates, ALC/GPC 150C) with polystyrene columns (Showa Denko K. K., AD806M/S) at 140ºC using *o*-dichlorobenzene (ODCB) as a solvent. The stereostructure of polypropylene was determined by ^{13}C NMR (Bruker 400 MHz) at 120ºC using 1,2,4-trichlorobenzene as a diluent and 1,1,2,2-tetrachloroethane-d_2 as an internal lock and reference.

2.2.5 Statistical analysis of polymer

The stereostructure of polypropylene was analyzed based on a two-sites model, where chain-end control[31] and enantiomorphic-site control statistics were assumed.[32] Even though a three-sites model gives more rigorous interpretation for the streostructure of polypropylene, this model requires information of longer stereo sequences, i.e. higher magnetic field in NMR.[3] For usual pentad sequences, the two-sites model was rather suitable.[32] In the two-sites model, *mmmm* is expressed as follows,

$$mmmm = \omega\{\sigma^5 + (1-\sigma)^5\} + (1-\omega)P_m^4$$

Here, σ is the probability to select a d-unit in the enantiomorphic-site model. P_m is the probability to select a meso diad configuration in the chain-end control model. ω is the weight ratio between the chain-end control model and enantiomorphic-site model. The other pentad sequences were similarly derived. The three parameters (σ, P_m, ω) were numerically optimized in order to fit experimental pentad sequences of polypropylene.

2.2.6 UV-vis diffuse reflectance spectroscopy (DRS) of catalyst

UV-vis DR spectra of the catalysts were acquired on a JASCO V-670 spectrophotometer equipped with integrating sphere. Catalyst powder was put into a quartz cell under nitrogen atmosphere. The DR spectra were recorded between 350 and 650 nm with a resolution of 1 nm and $BaSO_4$ was used as a background.

2.3 Results and Discussion

The prepared catalysts were characterized by UV-vis DRS as shown in Figure 1, together with the reference spectra of the homogeneous complexes diluted in toluene. Cp_2TiCl_2 in toluene exhibited two absorption bands (Figure 1(a)), where the higher and lower energy bands are respectively assigned as ligand-to-metal charge transfer (LMCT) for Cp $\rightarrow$ Ti and Cl $\rightarrow$ Ti.[33] On the other hand, $CpTiCl_3$ in toluene showed a single absorption band at 406 nm. Though Hamar et al. reported the presence of a weak shoulder at 475 nm (in dichloromethane),[34] we could not observe it probably due to its small oscillation strength. Upon physical immobilization, the lower energy band of Cp_2TiCl_2 (Cp $\rightarrow$ Ti) shifted hypsochromically, while the higher energy band was hardly shifted though its intensity was greatly reduced in immobilization. A hypsochromic shift usually occurs when the electron density of a metal center increases.[35,36] Electron withdrawal upon immobilization on $MgCl_2$ arises from the coordination of Cl ligands of a complex to surface Lewis acidic Mg sites (while electron donation arises from the coordination of electron-rich Cl of $MgCl_2$ to a metal center).[37] On the contrary, the spectrum of $CpTiCl_3/MgCl_2$(P) was rather complicated: the strongest absorption appeared at 485 nm, whose position was completely different from the original one, and two weak shoulders were also observed at around 410 and 450 nm.

Although the origins of these bands are unclear yet, the spectral variations upon immobilization suggest stronger interaction of $CpTiCl_3$ with $MgCl_2$ than that of Cp_2TiCl_2. The direct characterization of the electron density of the Ti center using X-ray photoemission

spectroscopy was unsuccessful for the scare Ti concentrations. The chemical immobilization of the two complexes in the presence of TEA has brought about the intensification of absorption below 400 nm, which is known as a result of alkylation.[38-40]

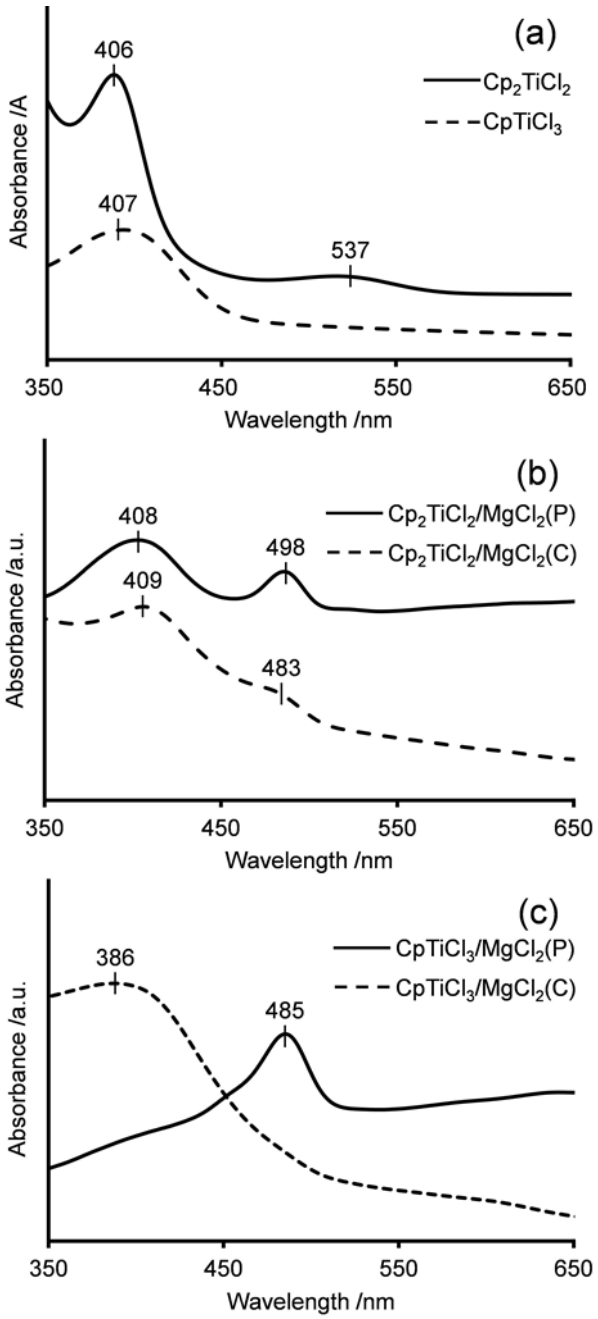

Figure 1. UV-vis spectra of non-supported and supported Cp_xTiCl_{4-x}. (a) Cp_2TiCl_2 and $CpTiCl_3$ in toluene; (b) $Cp_2TiCl_2/MgCl_2$; (c) $CpTiCl_3/MgCl_2$.

Propylene homopolymerization was conducted with the prepared $Cp_xTiCl_{4-x}/MgCl_2$ catalysts combined with MMAO or TEA activator. Table 2 summarizes the polymerization results together with the results for the homogeneous Cp_xTiCl_{4-x} and heterogeneous $TiCl_4/MgCl_2$ catalysts.

Table 2. Propylene polymerization results[a]

Catalyst	Activator	Activity (kg-PP·mol-Ti^{-1}·atm^{-1}·h^{-1})	*mmmm* (mol%)	*rrrr* (mol%)	M_n x 10^{-4} (g·mol^{-1})	M_w/M_n
$Cp_2TiCl_2/MgCl_2$(P)	MMAO	77.7	1.8	10.5	1.7	4.4
	TEA	9.1	48.8	3.7	2.0	5.1
$CpTiCl_3/MgCl_2$(P)	MMAO	76.3	2.1	10.5	3.3	3.3
	TEA	6.0	43.9	5.3	1.9	6.9
$TiCl_4/MgCl_2$(P)	MMAO	670.0	42.0	5.7	2.4	8.4
	TEA	824.0	45.6	6.9	2.3	8.6
$Cp_2TiCl_2/MgCl_2$(C)	MMAO	42.6	3.1	10.2	1.4	4.7
	TEA	33.8	48.2	4.2	2.0	4.6
$CpTiCl_3/MgCl_2$(C)	MMAO	74.4	41.6	6.4	3.1	9.8
	TEA	61.2	49.5	6.1	2.4	9.1
$TiCl_4/MgCl_2$(C)	MMAO	142.2	41.5	7.4	3.4	12.4
	TEA	98.4	39.2	7.8	1.9	10.3
Cp_2TiCl_2	MMAO	56.9	1.5	11.2	0.9	5.3
$CpTiCl_3$	MMAO	11.7	1.4	9.6	4.1	2.6

[a] Solvent: 200 mL of toluene, activator: MMAO (20 mmol·L^{-1}) or TEA (10 mmol·L^{-1}), Al/Ti molar ratio: 500, propylene pressure: 5 atm, temperature: 40°C, and polymerization time: 30 min.

Cp_xTiCl_{4-x} physically supported on $MgCl_2$ had higher activities than the corresponding homogeneous complexes when activated by MMAO. The degree of the activation induced by the immobilization on $MgCl_2$ was much larger for $CpTiCl_3$. Reduction and subsequent dimerization of Ti(IV) to inactive species represents the most probable explanation for rapid deactivation and low activities of homogeneous Cp_xTiCl_{4-x}.[41] The stabilization of active species upon immobilization on $MgCl_2$ accounts for the observed activity enhancements. On the other hand, the activities of $Cp_xTiCl_{4-x}/MgCl_2$(P) were much lower than that of $TiCl_4/MgCl_2$(P). The leaching of Ti components actually happened when the catalysts were treated with MMAO in the absence of donors. However, typical leaching amounts corresponding to 10-25% of the Ti contents in the catalysts were too low to explain the observed activities. Polypropylene made by $Cp_xTiCl_{4-x}/MgCl_2$(P) was atactic, as in homogeneous Cp_xTiCl_{4-x}. Such a stereostructure is generally obtained under chain-end controlled polymerization under negligible steric restriction from an active site,[42,43] as was affirmed by the insensitivity of the polypropylene stereostructure to the number of Cp ligands (Table 2). TEA as an activator led to much lower activities of $Cp_xTiCl_{4-x}/MgCl_2$(P) compared with MMAO, producing moderately isotactic polypropylene bearing non-negligible *rrrr* fractions. Such a stereostructure of polypropylene is typical for

traditional Ziegler-Natta catalysts without donor.[44] The stereostructures of polypropylene produced with Cp_xTiCl_{4-x}/MgC_2(P) were completely different between TEA and MMAO, which clearly indicates that the kind of activator affected the kind of active sites formed.

The chemically supported Cp_2TiCl_2 and $CpTiCl_3$ catalysts activated with MMAO respectively had lower and higher activities than the corresponding homogeneous complexes. The obtained polypropylene was atactic for $Cp_2TiCl_2/MgCl_2$(C), while moderately isotactic for $CpTiCl_3/MgCl_2$(C). When TEA was used as an activator, $Cp_xTiCl_{4-x}/MgCl_2$(C) had much higher activities than $Cp_xTiCl_{4-x}/MgCl_2$(P), producing similarly isotactic polymer. These results indicated that the preparation method also affected the kind of active sites and the chemical treatment with TEA upon immobilization led to an environment in which isospecific active sites were more easily formed (whose origin is described later).

The molecular weight (M_n) and molecular weight distribution (M_w/M_n) of the obtained polypropylene are listed in Table 2. M_n of moderately isotactic polypropylene ranged from 1.9-3.4 x 10^4 g/mol without a clear tendency. On the other hand, M_w/M_n became narrower with the increase in the number of Cp ligands for both of the preparation methods. The bulky Cp ligand is likely to suppress the formation of agglomerated Ti species on $MgCl_2$ during polymerization and

consequently reduce the expansion of the active site heterogeneity.[45] Moderately isotactic polypropylene produced from $Cp_xTiCl_{4-x}/MgCl_2$(C) had broader M_w/M_n compared with $Cp_xTiCl_{4-x}/MgCl_2$(P) except $Cp_2TiCl_2/MgCl_2$. It was inferred that supported $Cp_2TiCl_2/MgCl_2$ is more tolerant to the heterogenization (reduction as well as agglomeration) induced by TEA during catalyst preparation.

The stereostructure of polypropylene was analyzed based on the two-sites model in order to examine mechanisms of stereoselective polymerization of propylene with the different catalysts. The results of the fitting are shown in Table 3. In the case of moderately isotactic polypropylene, the calculated pentad values coincided well with the experimental values. The σ values were around 0.9 and not dependent on the kinds of activators, preparation methods, and precursor structures. This fact indicates that all the moderately isotactic polymers were formed at active sites with very similar steric environments. The active site structure in traditional Ziegler-Natta catalysts is well known as trivalent neutral Ti species situated in a pseudo octahedral symmetry having one vacant site for monomer coordination.[3,4,46-49] Accordingly, it is natural to assume that trivalent neutral active species were formed during polymerization when the moderately isotactic polymers were obtained. It means that supported Cp_xTiCl_{4-x} might be converted into

trivalent neutral species upon the contact with an activator either during catalyst synthesis or during polymerization. On the contrary, P_m decreased (i.e. the syndiospecificity of the chain-end controlled model increased) when the number of Cp ligands decreased and when the chemical preparation method was used. It seemed that P_m became lower for a condition in which the reduction of titanium chloride was more facile: a smaller number of Cp ligands leads to easier reduction of the Ti center, the chemical preparation method includes treatment with TEA, and TEA as an activator is a stronger reducing agent than MMAO. All these factors led to lower P_m values. In the case of atactic polypropylene produced from supported Cp_xTiCl_{4-x}, the fitting based on the two-sites model automatically gave $\omega = 0$, indicating that polymerization totally obeys the chain-end controlled mechanism. However, as shown in the large χ^2 values, the fitting degrees were much lower for the atactic polypropylene. The fitting degrees were never improved by adding another chain-end controlled model, indicating that a multisite nature of active sites could not account for the deviation. It is believed that either the enantiomorph of active sites or the stereo configuration before the last insertion exerts a secondary influence on the chain-end controlled polymerization. The values of P_m became almost the same as those for the unsupported catalysts, resulting in a hypothesis that active sites giving atactic polypropylene might be identical

to those for the unsupported metallocene catalysts, i.e. tetravalent cationic Ti species in a pseudo tetrahedral symmetry.

Table 3. Fitting results for the stereostructure of polypropylene using the two-sites model

Catalyst	Activator	σ	P_m	Ω	$\chi^{2\,a}$	Calc. *mmmm*[b] (mol%)	Calc. *rrrr*[b] (mol%)
$Cp_2TiCl_2/MgCl_2$(P)	MMAO	-	0.40	0	94	2.7	12.7
	TEA	0.91	0.38	0.79	21	48.9	3.8
$CpTiCl_3/MgCl_2$(P)	MMAO	-	0.40	0	78	2.6	13.0
	TEA	0.91	0.36	0.71	9.1	44.0	5.4
$TiCl_4/MgCl_2$(P)	MMAO	0.89	0.33	0.75	8.3	42.1	5.7
	TEA	0.91	0.30	0.74	14	45.7	6.9
$Cp_2TiCl_2/MgCl_2$(C)	MMAO	-	0.41	0	51	2.9	12.0
	TEA	0.90	0.32	0.84	8.4	48.3	4.2
$CpTiCl_3/MgCl_2$(C)	MMAO	0.90	0.34	0.70	7.3	41.7	6.4
	TEA	0.91	0.27	0.80	21	49.6	6.2
$TiCl_4/MgCl_2$(C)	MMAO	0.89	0.28	0.75	8.1	41.6	7.4
	TEA	0.87	0.25	0.78	22	39.3	8.0
Cp_2TiCl_2	MMAO	-	0.41	0	119	2.7	12.4
$CpTiCl_3$	MMAO	-	0.40	0	162	2.58	12.89

[a] $\chi^2 = \sum\{(\text{exp.}-\text{calc.})^2 \cdot \text{error}^{-2}\}$

[b] Calculated based on the optimized parameters.

In order to further examine the nature of active sites, CMDMS was added as a probe in propylene polymerization. An external donor would improve the isospecificity of Ziegler-Natta type active sites (trivalent neutral Ti species), while it would not affect the stereospecificity of metallocene type active sites (tetravalent cationic Ti species). Results of polymerization are shown in Table 4.

Table 4. Results of propylene polymerization with external donor [a]

Catalyst	Activator	Al/CMDMS (mol·mol^{-1})	Activity (kg-PP·mol-Ti^{-1}·atm^{-1}·h^{-1})	*mmmm* (mol%)
$Cp_2TiCl_2/MgCl_2$(P)	MMAO	20	11.7	1.8
	TEA	10	3.5	72.8
$CpTiCl_3/MgCl_2$(P)	MMAO	20	1.2	4.9
	TEA	10	None	
$TiCl_4/MgCl_2$(P)	MMAO	20	3.3	61.2
	TEA	10	409.8	79.8
$Cp_2TiCl_2/MgCl_2$(C)	MMAO	20	3.2	3.4
	TEA	10	19.6	72.4
$CpTiCl_3/MgCl_2$(C)	TEA	10	31.2	74.7
$TiCl_4/MgCl_2$(C)	TEA	10	34.5	66.0

[a] Solvent: 200 mL of toluene, activator: MMAO (20 mmol·L^{-1}) or TEA (10 mmol·L^{-1}), Al/Ti molar ratio: 500, propylene pressure: 5 atm, temperature: 40ºC, polymerization time: 30 min.

The addition of CMDMS decreased the catalyst activities, which was much more prominent for MMAO due to strong Lewis acid-base interaction. When CMDMS was added under conditions which had produced moderately isotactic polypropylene in the absence of donors (see Table 2), the isotacticity of polypropylene was improved, irrespective of the kinds of the precursors and

preparation methods. On the contrary, the stereoregularity of polypropylene was not changed by the addition of CMDMS for aspecific active sites. These results are consistent with our hypothesis mentioned above. From a viewpoint of the charge state of active sites, the activity of metallocene type active sites should increase in polar solvents.[50] Propylene polymerization activities were compared in less polar toluene and in more polar dichloromethane (Table 5).

Table 5. Effects of solvent on polymerization activity[a]

Catalyst	Activator	Solvent	Activity (kg-PP·mol-Ti^{-1}·atm^{-1}·h^{-1})
$Cp_2TiCl_2/MgCl_2$(C)	MMAO	Toluene	42.6
	MMAO	Dichloromethane	429.1
	TEA	Toluene	33.8
	TEA	Dichloromethane	38.2
$TiCl_4/MgCl_2$(P)	MMAO	Toluene	670.2
	MMAO	Dichloromethane	267.2
	TEA	Toluene	824.0
	TEA	Dichloromethane	59.1
Cp_2TiCl_2	MMAO	Toluene	56.9
	MMAO	Dichloromethane	456.6

[a] Solvent: 200 mL of toluene or dichloromethane, activator: MMAO (20 mmol·L^{-1}) or TEA (10 mmol·L^{-1}), Al/Ti molar ratio: 500, propylene pressure: 5 atm, temperature: 40ºC, and polymerization time: 30 min.

As expected, the activities of the homogeneous catalysts became much higher in dichloromethane. On the contrary, the activities of heterogeneous $TiCl_4/MgCl_2$(P) decreased regardless of the activators in dichloromethane. The activity of $Cp_2TiCl_2/MgCl_2$(C) increased in dichloromethane when activated by MMAO, while this was not the case for TEA. This result is highly consistent

with our hypothesis that the isospecific active sites are trivalent neutral species and the aspecific active sites are tetravalent cationic species. However, it is not clear how isospecific active sites of trivalent neutral species were formed. Considering that the stereospecificity of isospecific active sites was almost the same for the different precursors, Cp ligands might be removed to form trivalent neutral species. In order to clarify the mechanism of active sites formation and structure of active sites, further analysis is required.

Based on the results and discussion, we propose that the reduction of Cp_xTiCl_{4-x} supported on $MgCl_2$ by alkylaluminum leads to the formation of Ziegler-Natta type isospecific active sites, and that the ease of the reduction depends on the type of homogeneous precursors, the catalyst preparation method and the kind of activators. Since these isospecific active sites are never formed for homogeneous Cp_xTiCl_{4-x}, it can be concluded that a role of $MgCl_2$ is to stabilize reduced Cp_xTiCl_{4-x} as isospecific active sites.

Propylene polymerization results using $LTiCl_3/MgCl_2(C)$ were shown in Table 6.

Table 6. Propylene polymerization results[a]

Catalyst	Activator	Activity (kg-PP·mol-Ti^{-1}·atm^{-1}·h^{-1})	*mmmm* mol%	*rrrr* mol%
$CpTiCl_3/MgCl_2(C)$	MMAO	74.4	41.6	6.4
	TEA	61.2	49.5	6.1
$IndTiCl_3/MgCl_2(C)$	MMAO	79.6	42.6	6.6
	TEA	43.5	48.3	6.5
$Cp^*TiCl_3/MgCl_2(C)$	MMAO	53.5	2.8	14.3
	TEA	14.0	44.7	5.5
$IndTiCl_3$	MMAO	231.2	2.8	10.0
Cp^*TiCl_3	MMAO	663.4	2.0	15.3

$Cp^*TiCl_3/MgCl_2(C)$ produced mostly atactic PP in the presence of MMAO. However, $CpTiCl_3/MgCl_2(C)$ and $IndTiCl_3/MgCl_2(C)$ produced relatively isotactic PP by MMAO. When TEA was used, the activity was increased in the order of $Cp^*TiCl_3/MgCl_2(C)$ < $IndTiCl_3/MgCl_2(C)$ < $CpTiCl_3/MgCl_2(C)$. This activity trend was opposite to homogeneous catalyst systems. From these results, the reduction of titanocene during catalyst preparation and/or polymerization by

alkylaluminum leads to the formation of Ziegler-Natta type isospecific active sites. The ease of the reduction depended on the type of precursors, the catalyst preparation method and the kind of activators.

2.4 Conclusion

The active site natures of $MgCl_2$-supported Cp_2TiCl_2 and $CpTiCl_3$ catalysts were investigated for propylene polymerization and compared with those of non-supported complexes and traditional Ziegler-Natta catalysts. It was found that the catalyst preparation method and the kind of activators affect the formation of different types of active sites. $Cp_2TiCl_2/MgCl_2$ and $CpTiCl_3/MgCl_2$ catalysts formed active sites identical to those of a $TiCl_4/MgCl_2$ catalyst when activated by TEA, and produced isotactic polypropylene, whose stereoregularity was enhanced by the addition of a donor. On the other hand, the usage of MMAO tended to form aspecific active sites similar to those of the non-supported complexes, whose activities were dramatically improved in polar dichloromethane. The isospecific active sites were assigned as neutral Ti(III) stabilized by a $MgCl_2$ support, while aspecific active sites were cationic Ti(IV). Thus, we found novel dual active site natures of $MgCl_2$-supported titanocene catalysts, which can be switched by the kind of activator.

Reference

[1] P. Corradini, V. Busico, L. Cavallo, G. Guerra, M. Vacatello, V. Venditto, *J. Mol. Catal* **1992**, *74*, 433.

[2] M. A. Giardello, M. S. Eisen, C. L. Stern, T. J. Marks, *J. Am. Chem. Soc*. **1995**, *117*, 12114.

[3] V. Busico, R. Cipullo, G. Monaco, G. Talarico, M. Vacatello, J. C. Chadwick, A. L. Segre, O. Sudmeijer, *Macromolecules* **1999**, *32*, 4173.

[4] B. Liu, T. Nitta, H. Nakatani, M. Terano, *Macromol*. *Chem*. *Phys*. **2002**, *203*, 2412.

[5] X. Yang, C. L. Stern, T. J. Marks, *J. Am. Chem. Soc*. **1991**, *113*, 3623.

[6] R. F. Jordan, C. S. Bajgur, R. Willett, B. Scott,. *J. Am. Chem. Soc.* **1986**, *108*, 7410.

[7] K. Soga, M. Kaminaka, *Makromol*. *Chem*. **1993**, *194*, 1745.

[8] S. Paavola, T. Saarinen, B. Lofgren, P. Pitkanen, *Polymer* **2004**, *45*, 2099.

[9] M. Chang, *U.S. Patent 4925821*, **1990**.

[10] T. Takahashi, *U.S. Patent* 5026797, **1991**

[11] E. I. Iiskola, S. Timonen, T. T. Pakkanen, O. Harkki, P. Lehmus, J. V. Seppala, *Macromolecules* **1997**, *30*, 2853.

[12] H. Schneider, G. T. Puchta, F. A. R. Kaul, G. Raudaschl-Sieber, F. Lefebvre, G. Saggio, D. Mihalios, W. A. Herrmann, J. M. Basset, *J. Mol. Catal. A* **2000**, *170*, 127.

[13] F. Bortolussi, J. P. Broyer, R. Spitz, C. Boisson, *Macromol. Chem. Phys.* **2002**, *203*, 2501.

[14] J. Tian, Y. Soo-Ko, R. Metcalfe, Y. Feng, S. Collins, *Macromolecules* **2001**, *34*, 3120.

[15] Y. Giannini, *Makromol. Chem. Suppl.* **1981**, *5*, 216.

[16] T. Keii, E. Suzuki, M. Tamura, M. Murata, Y. Doi, *Makromol. Chem.* **1982**, *183*, 2285.

[17] N. Kashiwa, J. Yoshitake, *Makromol. Chem., Rapid Commun.* **1983**, *4*, 41.

[18] G. D. Bunkatov, S. H. Sheplev, V. A. Zakharov, S. A. Sergeev, Y. I. Yermakov, *Makromol. Chem.* **1982**, *183*, 2657.

[19] G. Satyanarayana, S. Sivaram, *Macromolecules* **1993**, *26*, 4712.

[20] M. Kaminaka, K. Soga, *Makromol. Chem., Rapid Commun.* **1991**, *12*, 367.

[21] K. Soga, Y. Suzuki, T. Uozumi, E. Kaji, *J. Polym. Sci., Part A: Polym. Chem.* **1997**, *35*, 291.

[22] N. Ishihara (Idemitsu Kosan Co. Ltd.), *Jpn H06-080720*, **1994**.

[23] J. R. Severn, J. C. Chadwick, *Macromol. Chem. Phys.* **2004**, *205*, 1987.

[24] J. R. Severn, J. C. Chadwick, *Macromol. Rapid Commun.* **2004**, *25*, 1024.

[25] R. Huang, R. Duchateau, C. E. Koning, J. C. Chadwick, *Macromolecules* **2008**, 41, 597.

[26] W. Ochedzan-Siodłak, M. Nowakowska, *Eur Polym. J.* **2005**, *41*, 941.

[27] Z. Guan, Y. Zheng, S. Jiao, *J. Mol. Catal. A* **2002**, *188*, 123.

[28] A. Conte, M. F. V. Marques, *Eur Polym. J.* **2001**, *37*, 1887.

[29] J. Jin, C. Ahn, T. Sano, T. Uozumi, M. Murata, H. Ozaki, H. Hagihara, *J. Polym. Sci., Part A: Polym. Chem.* **2000**, *38*, 3355.

[30] K. K. Kang, J. K. Oh, Y. Jeong, T. Shiono, T. Ikeda, *Macromol. Rapid Commun.* **1999**, *20*, 308.

[31] F. A. Bovey, G. V. D. Tiers, *J. Polym. Sci.* **1960**, *44*, 173.

[32] Y. Inoue, Y. Itabashi, R. Chujo, Y. Doi, *Polymer* **1984**, *25*, 1640.

[33] M. R. M. Bruce, A. Kenter, D. R. *J.* Tyler, *Am. Chem. Soc.* **1984**, *106*, 639.

[34] J. W. Kenney, D. R. Boone, D. R. Striplin, Y. H. Chen, K. B. Hamer, *Organometallics* **1993**, *12*, 3671.

[35] N. I. Makela, H. R. Knuuttila, M. Linnolahti, T. A. Pakkanen, M. A. Leskela, *Macromolecules* **2002**, *35*, 3395.

[36] P. Carrion, F. Carrillo-Hermosilla, C. Alonso-Moreno, A. Otero, A. Antinolo, J. Sancho, E. Villasenor, *J. Mol. Catal. A*: *Chem.* **2006**, *258*, 236.

[37] T. Taniike, M. Terano, *Macromol. Rapid Commun.* **2007**, *28*, 1918.

[38] D. Coevoet, H. Cramail, A. Deffieux, *Macromol. Chem. Phys.* **1998**, *199*, 1451.

[39] D. Coevoet, H. Cramail, A. Deffieux, *Macromol. Chem. Phys.* **1998**, *199*, 1459.

[40] V. N. Panchenko, V. A. Zakharov, E. A. Paukshtis, *J. Mol. Catal. A*: *Chem.* **2005**, *240*, 33.

[41] J. C. W. Chien, *J. Am. Chem. Soc.* **1958**, 8*1*, 86.

[42] A. Zambelli, P. Locatelli, A. Provasoli, D. R. Ferro, *Macromolecules* **1980**, *13*, 267.

[43] J. A. Ewen, *J. Am. Chem. Soc.* **1984**, *106*, 6355.

[44] T. Hayashi, Y. Inoue, R. Chujo, Y. Doi, *Polymer* **1989**, *30*, 1714.

[45] T. Wada, T. Taniike, I. Kouzai, S. Takahashi, M. Terano, *Macromol. Rapid Commun.* **2009**, *30*, 887.

[46] T. Taniike, M. Terano, *J. Catal.* **2012**, *293*, 39.

[47] N. Kashiwa, J. Yoshikate, *Makromol. Chem.* **1984**, *185*, 1133.

[48] D. Fregonese, S. Mortara, S. Bresadola, *J. Mol. Cat. A*: *Chem.* **2001**, *172*, 89.

[49] A. S. N. Al-arifi, *J. Appl. Polym. Sci.* **2004**, *93*, 56.

[50] A. R. Siedle, W. M. Lamanna, R. A. Newmark, J. Stevens, D. E. Richardson, M. Ryan, *Makromol. Chem., Macromol. Symp.* **1993**, *66*, 215.

Chapter 3

UHV Preparation of $MgCl_2$ Active Surface for Ziegler-Natta Model Catalyst

3.1 Introduction

Solid catalysts are widely used in industrial processes. Since reaction takes place on surface of solid catalysts, understanding for several phenomena of solid surface is important. Ziegler-Natta catalyst is one of the most important solid catalysts, and is responsible for the production of more than 99% of the polypropylene in particular. $MgCl_2$-supported Ziegler-Natta catalysts consist of $TiCl_4$, $MgCl_2$, donors, triethylaluminum and H_2. The design of the structure of active sites is very important because active sites determine stereoregularity of polypropylene, molecular weight and molecular weight distribution. However, despite extensive efforts, there is still limited understanding of the nature of Ziegler-Natta catalysts, especially this is because of the nature of active sites. The multisite nature has inhibited the direct characterization of active sites, the evaluation of the catalytic performance of each active site, and the understanding of molecular-level behaviors of the catalysts. These heterogeneities are based on structure of $MgCl_2$.

In Ziegler-Natta catalysts, $MgCl_2$ is used as a support because $MgCl_2$ was found to show the highest activity among various solid carriers. The importance of the similarities in the crystal structures and ionic radii of $MgCl_2$ and $TiC1_4$ was pointed out by Kashiwa and Galli *et al.* Such a dramatic increase in activity was revealed to be caused by marked increases in the number of active species

(C*) as in well as the propagation rate constant (k_p). Improvements of C* and k_p were mainly based on high dispersion of the active titanium species on the large surface of $MgCl_2$ and increasing in the electron density on the active transition metal ion, which stabilizes the coordination of olefin monomer by back donation of an electron, respectively.

Bulk $MgCl_2$ exists as a two crystalline forms: the first one is α-$MgCl_2$ with the chloride anions organized in a face-centered cubic arrangement and the Mg cations in the octahedral interstices. It is more stable than β-$MgCl_2$ with the chloride anions organized in a hcp arrangement. Difference between two forms was only by the stacking of hexagonal layers: ABC BCA CAB • • • or ABC ABC ABC • • • for the α-$MgCl_2$ and β-$MgCl_2$, respectively. As for the support structure, the primary particles of activated $MgCl_2$ are composed of a few irregularly stacked Cl-Mg-Cl sandwiches. Terano et al. showed copresence of (100) and (110) lateral cuts by HR-TEM. For electroneutrality reasons, these two lateral cuts contain coordinatively unsaturated Mg^{2+} ions with coordination number 4 and 5 on the (110) and (100) cuts, respectively. $TiCl_4$ adsorbs on the $MgCl_2$ (110) surface only as saturated mononuclear species, while it can dimerize on the (100) surface. Busico et al. proposed that such dinuclear species was highly isospecific and mononuclear species was aspecific. Active sites of Ziegler-Natta catalysts are generally expressed

by Ti species situated in an octahedral symmetry as a result of adsorption on unsaturated $MgCl_2$ surfaces,[1] most plausibly on the (110) surface.[2-4] The internal donor plays an important role in controlling the amount and the distribution of Ti species on $MgCl_2$ surface. Donors interact with the Ti species in a non-bonded manner through coadsorption on $MgCl_2$ surfaces, so as to modulate the catalytic nature of the Ti species.[3,5,6] The catalytic nature of Ti species can be changed even during the elongation of one polymer chain due to ligand removal or exchange.[5] Molecular-level understandings have been gradually established as a result of huge knowledge accumulation. However, these understandings are inferred from the average data of the analysis results of polydispersity polymer and spectroscopic observations of heterogeneous catalyst surfaces. A number of solid catalysts more or less have similar problems relating to heterogeneity of catalyst surfaces.

One of the helpful ways to overcome these problems is surface science approach under ultra-high vacuum (UHV) condition. UHV surface science on metal substrates is such a way to directly obtain atomic-level information on surfaces. UHV studies on single crystal surfaces revealed a number of important surface phenomena, leading to new concepts in surface science. The instrumentation techniques developed for surface studies [12] include X-ray photoelectron

spectroscopy (XPS), low energy electron diffraction (LEED), auger electron spectroscopy (AES), secondary ion mass spectrometry (SIMS) and inelastic ion surface scattering (ISS) techniques.

For the Ziegler-Natta catalyst, Groups of Prof. Somorjai and Prof. Freund attempted to prepare well-defined Ziegler-Natta model surfaces under UHV condition.[9-11] However, the sublimation deposition of $MgCl_2$ on various metal substrates exhibited the dominant exposure of the chlorine-terminated (001) plane, which is known as inert for $TiCl_4$ and donor adsorption. Various reductive processes using Mg or electron bombardment were applied to enable $TiCl_4$ adsorption, such a reduction process is never implemented in usual preparation procedures of powder catalysts. However, chemical composition of prepared catalyst was $TiCl_4/TiCl_2/MgCl_2$ which was far from real catalyst.

Recent DFT calculations revealed that coordination of donors on unsaturated surfaces of $MgCl_2$ promotes the exposure of active surfaces, compared with the chlorine-terminated (001) surface.[8] It has been increasingly accepted that $MgCl_2$ support dynamically changes according to a given environment in the presence of coordinative molecules. This is relevant to the activation of $MgCl_2$ support for powder catalysts, which usually accompanies high-temperature treatment with a donor. It is also important that un-activated $MgCl_2$ hardly accepts the $TiCl_4$ adsorption. Based on all of

these backgrounds, objective of this section is that synthesis and characterization of $MgCl_2$ active surfaces which can be a precursor of Ziegler-Natta model surface having uniform structure prepared by donor-induced surface reconstruction. The model catalyst makes it possible to obtain molecular-level information on the surfaces of the Ziegler-Natta catalyst with direct experimental observation.

3.2 Experimental Section

Materials

Ar of G3 grade was used without further purification. Cu(110, diameter: 8 mm, thickness: 1 mm, 0.5acc) and Au(111, diameter: 8 mm, thickness: 1 mm, 0.5acc) were used as substrate. Pyridine, Tetrahydrofuran, and Ethyl benzoate (purchased from Kanto Chemical Co., Inc.) were dried using sodium. Spherical magnesium dichloride was used.

Instramental setup of Ultra-high vacuum (UHV) system

An UHV system is shown in Figure 3.1.

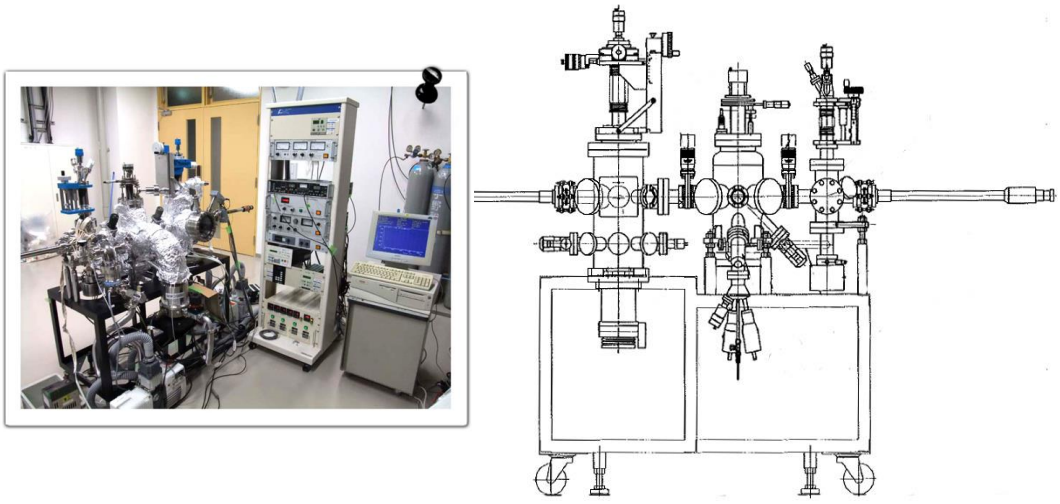

Figure 3.1. Picture and illustration of UHV system

The apparatus consisted of a preparation chamber, an analysis chamber, an evaporation chamber and an organic chamber maintained at background pressure of 1 x 10^{-9} Torr by turbo molecular pump. The sample under study was transferred from one chamber of the apparatus to the others through a series of gate valves and transfer arms.

Preparation chamber

The preparation chamber equipped with ISE 5 ion sputtering gun is used for surface cleaning. Figure 3.3 shows the designed heating system. A substrate was hung by a filament using a dip on its side face (Figure 3.2a), and attached to electrodes placed on the side parts of the holder (Figure 3.2b, c). A thermocouple connected to another set of electrodes (Figure 3.2b) was placed between the back face of the substrate and an alumina spacer (Figure 3.2c). These heating system achieve not only direct heating of the substrate through the filament but also direct measurement of the substrate temperature, thus leading to an accurate and quick temperature control, as shown in Figure 3.3. Stable ramping at a constant rate of 120 °C/min was easily achieved in the new system. This heating system was installed in two chambers for substrate cleaning and for $MgCl_2$ deposition & TPD experiments.

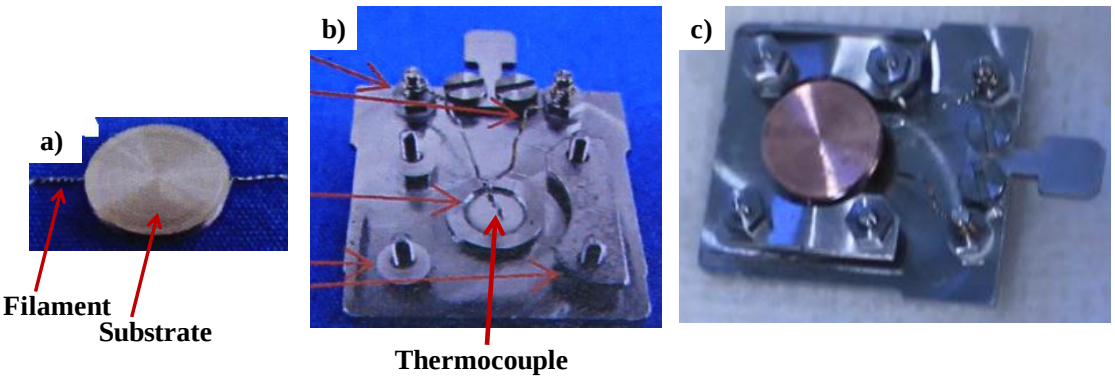

Figure 3.2. Pictures of the heating system

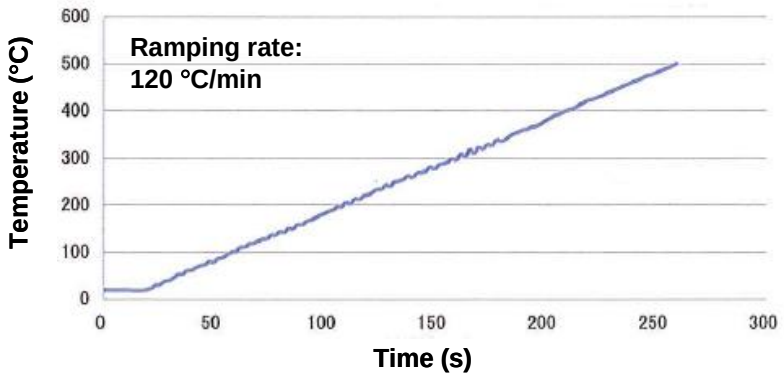

Figure. 3.3. Temperature ramping controlled at 120 °C/min in the new system

Evaporation chamber

UHV evaporator with integral flux monitor is equipped in the evaporation chamber. Graphite crucible is mounted inside the cell and the evaporation is achieved by mean of electron bombardment heating. Temperature of the source can be adjusted from the filament current and

electron energy, however we cannot measure the temperature directly. $MgCl_2$ bead is used as the deposition source. It is filled to the crucible under N_2 flow to prevent from moisture.

A sample translation system and a quadruple mass spectrometer (QMS) were also installed in the chamber for $MgCl_2$ deposition & TPD experiments (Figure 3.4 and 3.5). The translation system enables a sample to flip at 90^o for the $MgCl_2$ deposition and TPD experiments (Figure 3.5). The system enables to appropriately face the substrate surface toward the QMS detector at the closest position.

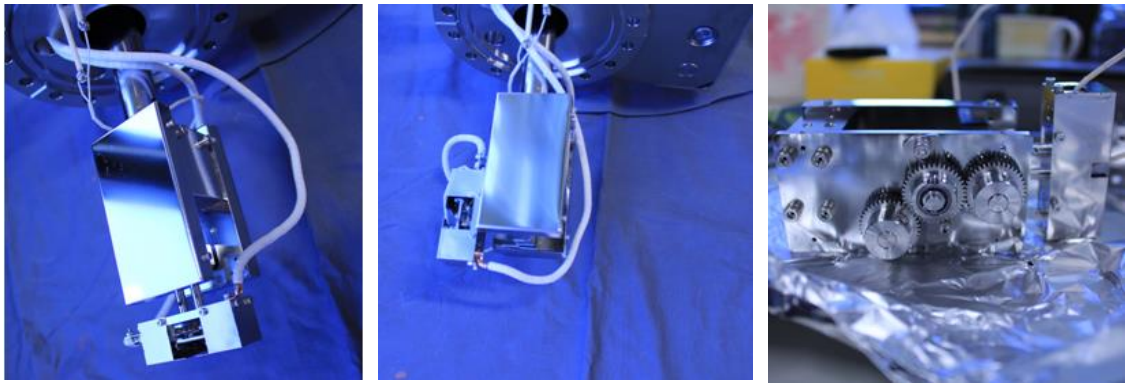

Figure 3.4. Pictures of the translation system

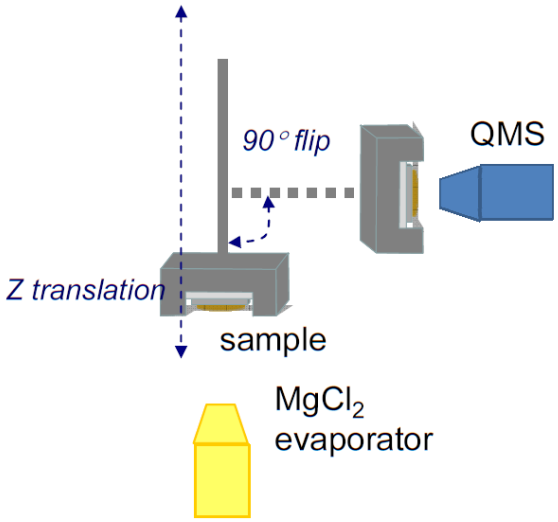

Figure 3.5. Illustrations of translation system

Analysis chamber

In the analysis chamber, electron analyzers (Low Energy Electron Diffraction: LEED and Auger Electron Spectroscopy: AES) were operated at fixed energy resolution.

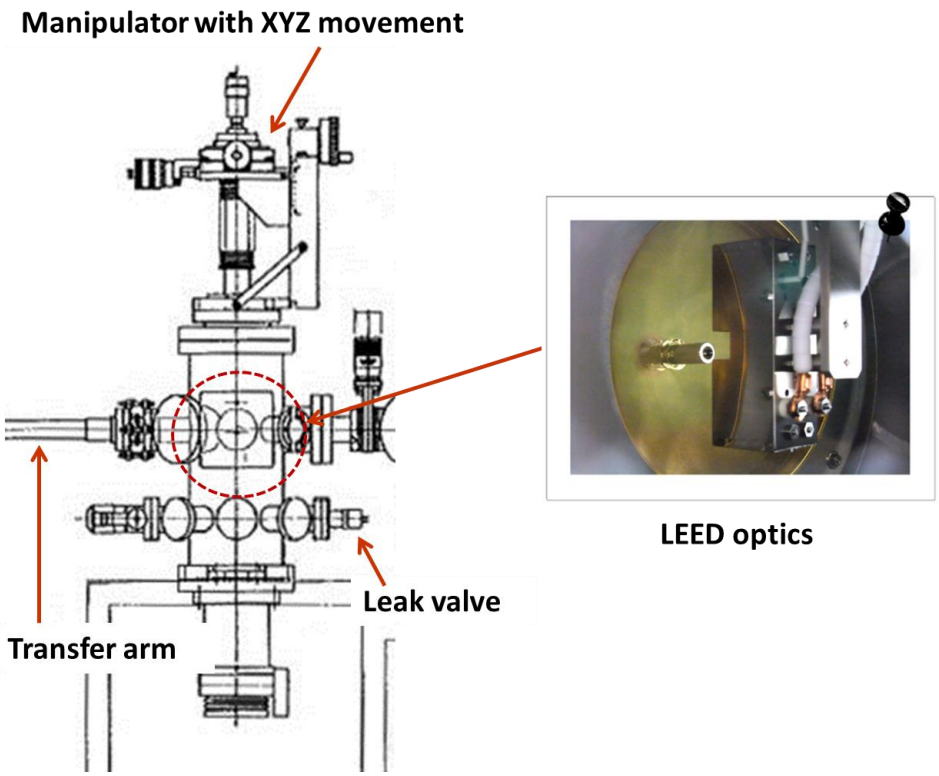

Figure 3.6. Illustrations of analysis chamber

Organic chamber

Organic chamber was connected to the preparation chamber across a gate valve. The organic chamber equips a line to dose organic molecules, a turbo molecular pump (TMP) which can operate at a relatively high pressure, a bypassing line to directly evacuate a great amount of dosed organic molecules with a rotary pump (RP), and a load-lock port for sample exchange or sample transfer to

outer instruments. It enables not only high-pressure dosing but also quick recovery to an UHV condition (~ 10^{-8} Torr) after dosing experiments.

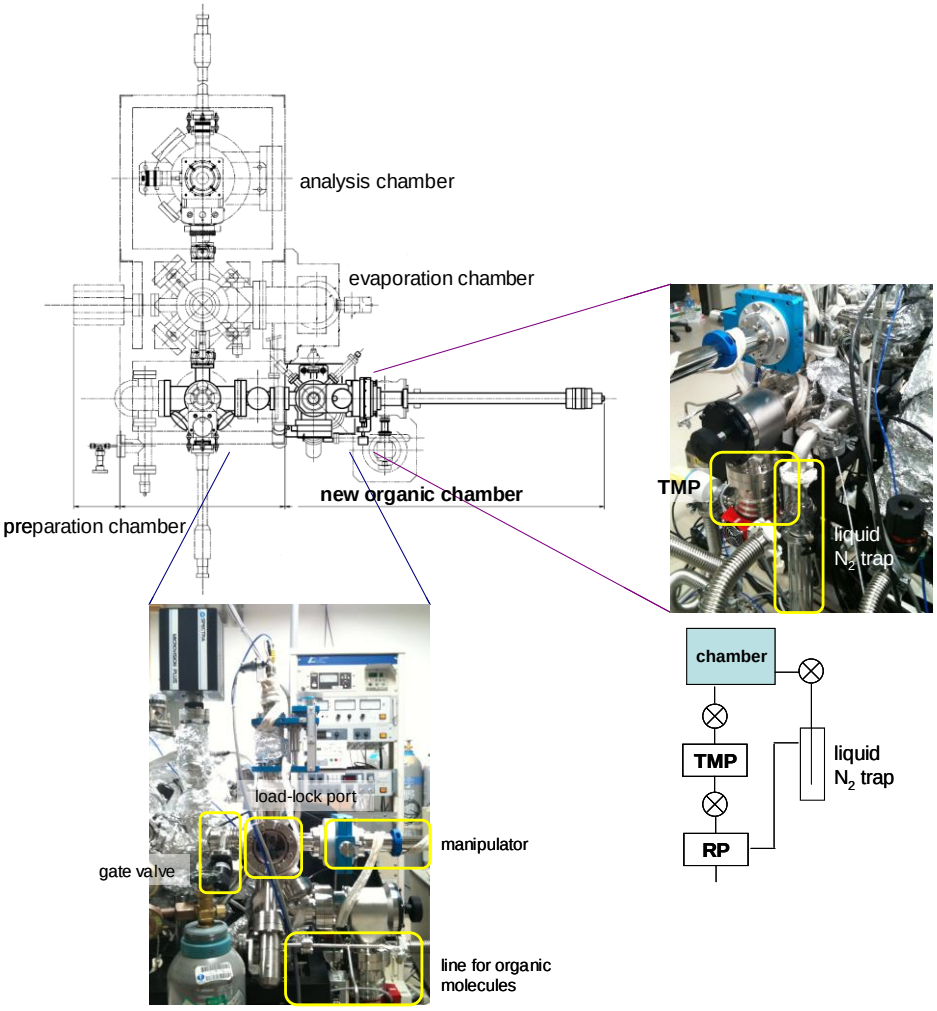

Figure 3.7. New chamber for introduction of organic molecules at saturated vapor pressure

3.3 Results and Discussion

3.3.1 Cleaning condition for Cu substrate

After setting up UHV system, Cu (110) substrate (1 cm^2 surface area) was set inside the chamber. The substrate was initially analyzed by AES and the spectrum is shown in Figure 3.7. The dominant peak at 270 eV indicates the carbon containing compound as the main contaminant. The surface cleaning condition was optimized by varying the Ar pressure from 5×10^{-6} Torr to 2×10^{-5} Torr at the energy range of 0.3 to 1.0 keV for sputtering time up to 30 min. At each condition, the cycle of Ar^+ sputtering and annealing at 500°C for 30 min was repeated 2 times before transferring the substrate to analyze the remaining carbon impurity in analysis chamber. AES analysis was conducted over several positions of the sample surface to confirm the cleanness. The effective cleaning was achieved at the conditions using Ar pressure 2×10^{-5} Torr at the energy of 1.0 keV for sputtering time 30 min. At this conditions, AES spectrum exhibits intense Cu MVV peak at 61 eV with no other contamination peak (as shown in blue line in Figure 3.7). LEED analysis was performed using low energy electron beam. The clear pattern of clean Cu substrate in Figure 3.8 indicates the absence of adatom of a well-ordered fcc (110) surface structure.

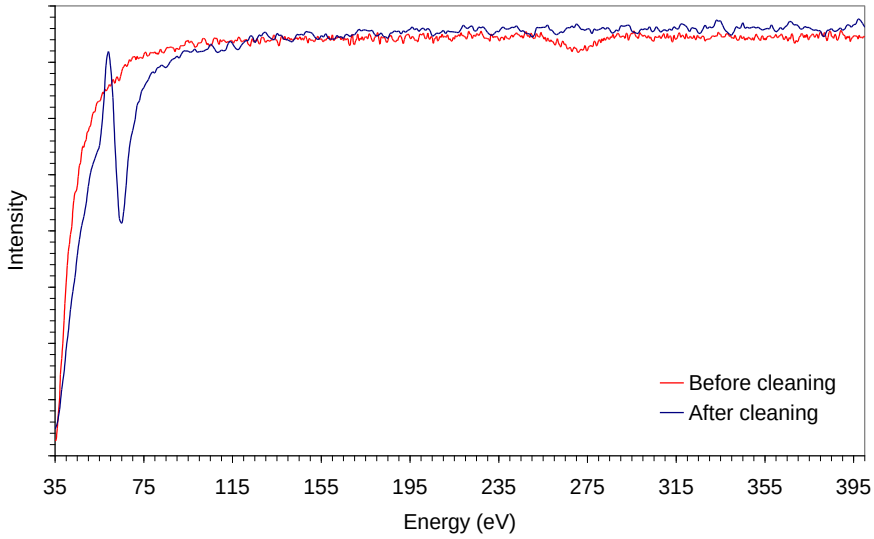

Figure 3.7. AES spectra of Cu (110) substrate before and after optimization of the cleaning condition

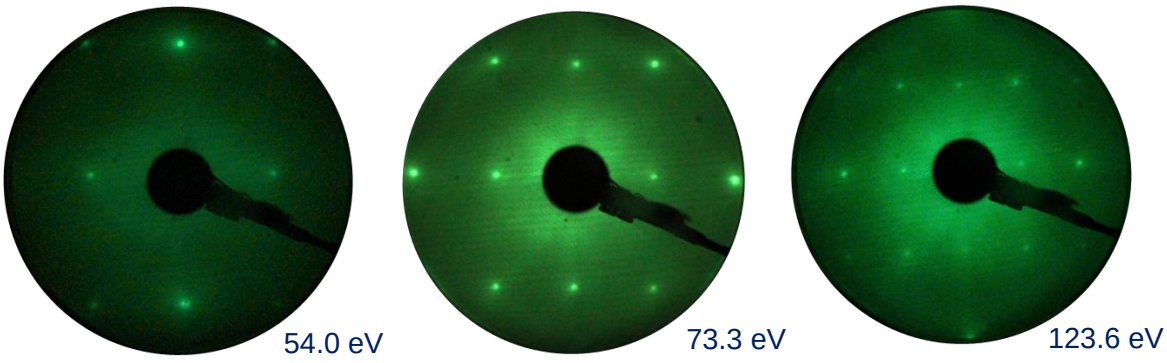

Figure 3.8. LEED pattern of clean Cu (110) substrate

3.3.2 Effects of deposition condition on $MgCl_2$ thickness

After obtaining the clean and ordered surface of Cu (110), the parameters for controlling film deposition such as deposition time, substrate temperature as well as kinetic energy of electron for bombardment heating of the $MgCl_2$ source were initially optimized.

As the thickness of the film is directly correlated to the deposition time, the deposition was carried out for 15 min by keeping the Cu (110) substrate surface at 40°C. The energy of electron for bombardment heating was kept at 900 eV in order to maintain identical $MgCl_2$ flux. After the deposition, $MgCl_2$ films were annealed at 300°C for 15 min in order to flatten the surface before analyzing the deposited film by AES and LEED.

Figure 3.9 exhibits the AES spectra of $MgCl_2$ film synthesized at 15 min deposition time. The peaks at 44 eV and 180 eV correspond to Mg LMM and Cl LVV, respectively. This indicates that the incident electrons have sufficient energy to generate heat allowing the sublimation of $MgCl_2$ source.

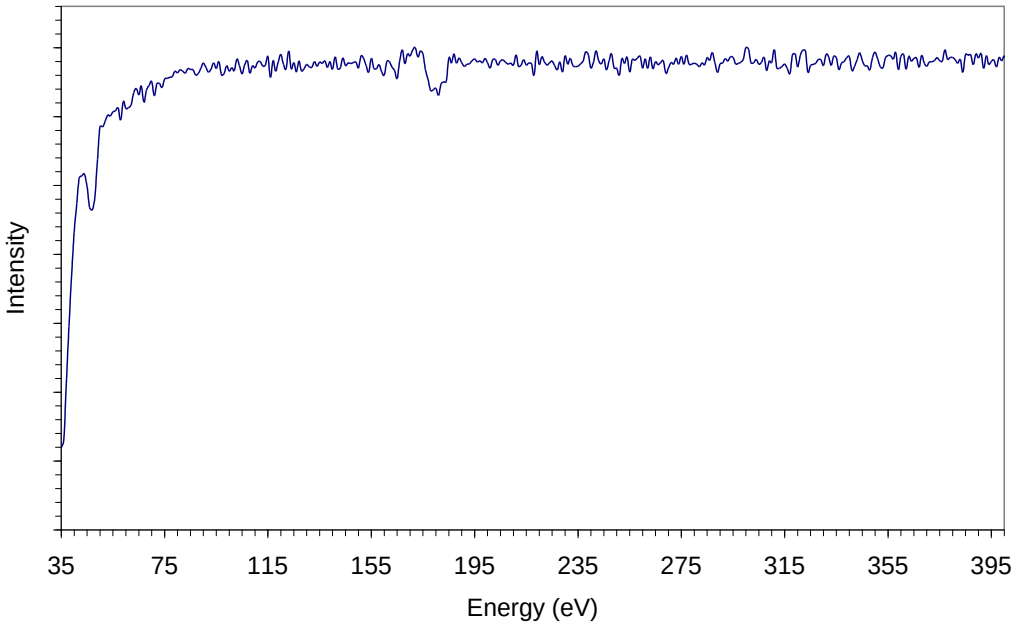

Figure 3.9. Auger electron spectroscopy of $MgCl_2$ film grown on Cu(110) at the deposition time 20 min.

The influence of substrate temperature and deposition time on the controlling of film growth was investigated as essential information to the subsequent experiments using donors. AES analysis was carried out in a short scan range (35-300 eV) with minimal acquisition time to minimize the damage of film. The AES spectra in Figure 3.10 showed that all $MgCl_2$ films deposited at the substrate temperature 60°C, 300°C and 350°C for the deposition time 10 min exhibited the presence of Mg at 44 eV, Cl at 180 eV and underlying Cu substrate at 61 eV.

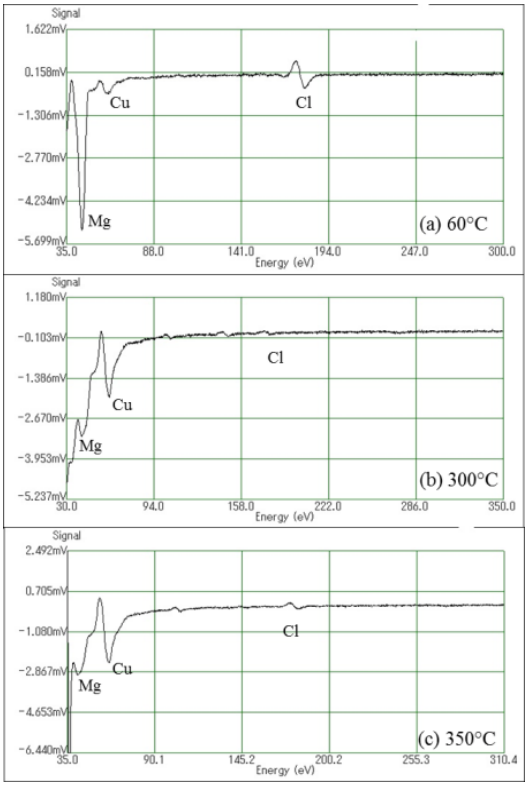

Figure 3.10. AES of $MgCl_2$ film obtained from 10 min deposition time on Cu(110) substrate held at (a) 60°C; (b) 300°C; and (c) 350°C The spectra were recorded using 1.5 keV primary beam energy.

The film thickness calculated using the following equation was 8.5, 4.4 and 2.8 Å for substrate temperature held at 60°C, 300°C and 350°C, respectively.

$$Cu_{MgCl_2}/Cu_{Clean} = e^{-d/\lambda_{Cu}}$$

Where

d: Over layer thickness (Å)

λ_{Cu}: Electron mean free path (Å)

Cu_{MgCl2}, Cu_{Clean}: Intensity of Cu peak

To increase the deposition time from 2 min to 80 min with the substrate temperature held at 60°C led to the decrease of Cu intensity and eventually it disappeared at 80 min. The thickness of film increased with the increase of time as shown in Figure 3.11. In contrast, AES spectrum of $MgCl_2$ film deposited at the substrate temperature held at 350°C remained unchanged after extending the deposition time, which suggests that there is a maximum coverage or thickness of $MgCl_2$ at the high substrate temperature. Somorjai et al. [13] reported a similar phenomenon for the deposition of $MgCl_2$ at an elevated substrate temperature. They concluded that the maximum coverage corresponded to the monolayer and excess $MgCl_2$ desorbed without getting sufficient interaction with the substrate.

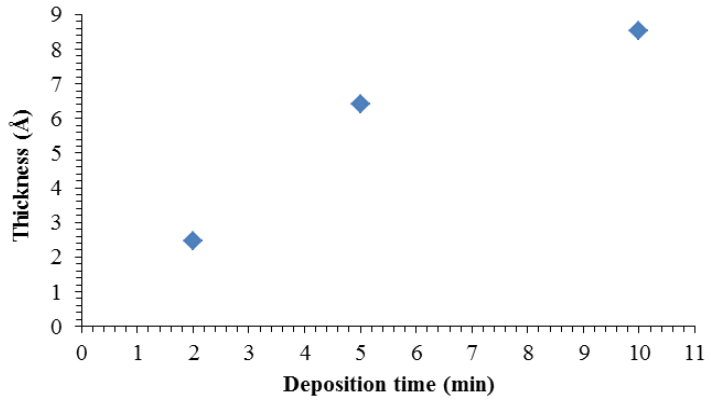

Figure 3.11. Relationship between $MgCl_2$ film thickness and deposition time at the substrate temperature 60°C.

In LEED analysis, clear hexagonal pattern can be obtained for the film deposited for 2 min (Figure 3.12b). Clear hexagonal patterns from LEED analysis indicated the formation of $MgCl_2$ films exposing the (001) basal plane. The thickness of film was estimated to be 2.5 Å, probably less than the value for perfect monolayer of $MgCl_2$. This suggested that the synthesis of $MgCl_2$ film within one monolayer coverage can be achieved by controlling the deposition time. As the coverage increased, diffuse spots appeared (Figure 3.12c) and at 5 min deposition time, LEED pattern exhibited 12 diffused spots surrounding the central (00)-spot due to the superposition of two 90° rotated hexagonal domains (Figure 3.13b). No change in LEED pattern was observed after annealing this film to 225°C and 275°C. Increasing the annealing temperature to 300°C led to the

decrease of film thickness from 6.4 Å (before annealing) to 3.1 Å and the higher ordered pattern was obtained (Figure 3.12e). The ratio between Mg intensity and Cl intensity from AES analysis remained unchanged within the experimental error range, indicating molecular desorption of $MgCl_2$ in the temperature range between 275-300°C. $MgCl_2$ film deposited for the deposition time above 10 min yielded no ordered structure (Figure 3.12d). The result that increase in the film thickness caused a rotational disorder in LEED images is consistent with the way of Van der Waals stacking of bulk $MgCl_2$ in the [001] direction; the ordered hexagonal pattern is a proof of a monolayer film, while the other LEED images came from multilayer films, which is in agreement with the estimated film thickness from AES analysis.

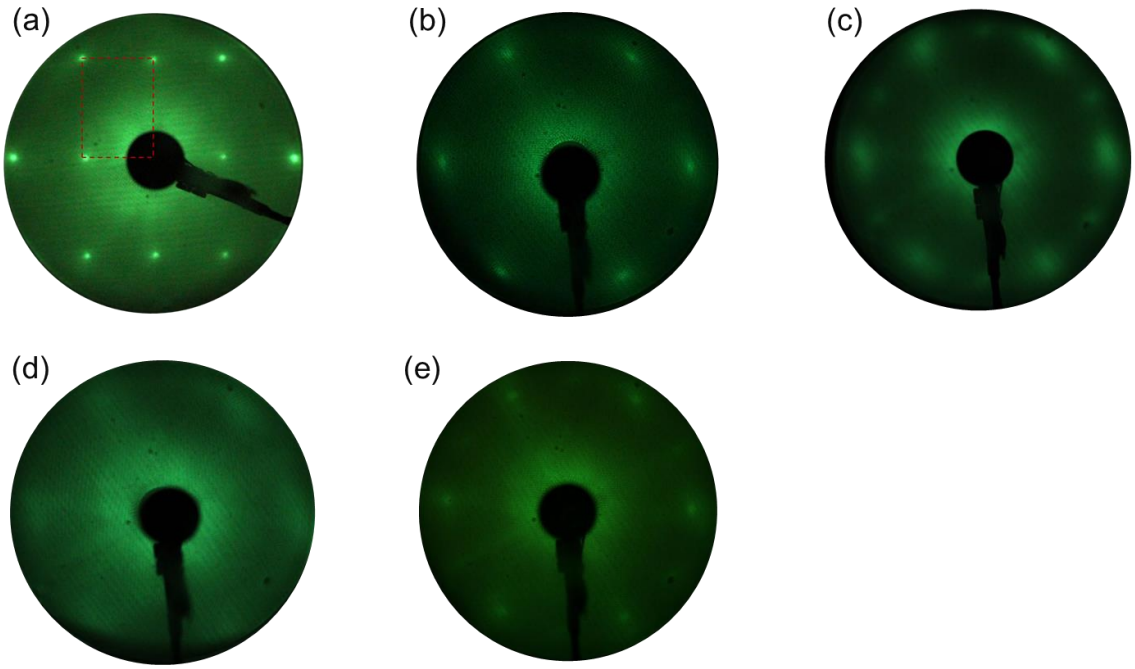

Figure 3.12. LEED patterns of (a) Cu(110) and $MgCl_2$ film deposited for (b) 2 min; (c) 5 min; (d) 10 min; and (e) after annealing $MgCl_2$ film deposited for 5 min at 300°C.

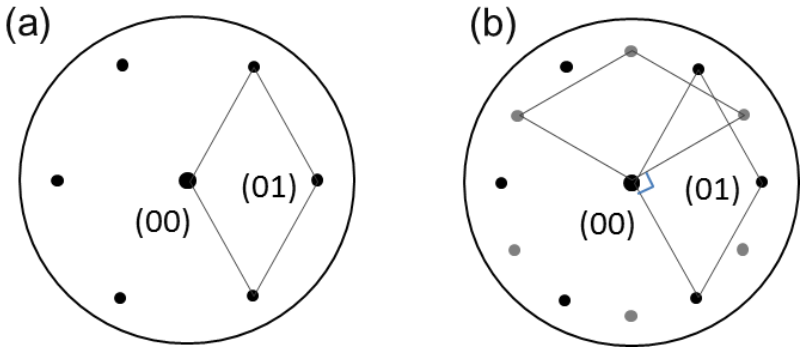

Figure 3.13. Illustration of LEED patterns of (a) monolayer $MgCl_2$ film and (b) bilayer $MgCl_2$ film.

3.3.3 Effects of geometric and chemical differences of the underlying substrates

The lattice constant of an $MgCl_2$ film estimated from a LEED pattern, 3.1 Å, was found to be abnormally smaller than that of the bulk, 3.64 Å, plausibly due to non-conformity of instrumental parameters. In order to solve this problem, a number of LEED patterns of monolayer $MgCl_2$ films on Cu(110) were systematically analyzed. As a result, the lattice constant of $MgCl_2$ monolayer films was calculated to be 3.41±0.06 Å. The reduction of the lattice constant from the bulk value is about 6%, which is frequently observed for atomically thin films. For example, Somorjai et al. have reported reduced lattice constants of $MgCl_2$ films. The compression depends on the underlying substrate and coverage, *e.g.* a monolayer $MgCl_2$ film deposited on Pt(111) gave the lattice constant of 3.34 Å due to strong influences of the substrate structure, while a multilayer film recovered back in the range of 3.6-3.7 Å [1].

In parallel to Cu(110), we have newly introduced Au(111) substrate for the comparative study. On the contrary to one-dimensional Cu (110), Au(111) is hexagonal, thus being suitable to compare the importance of the lattice structure on the synthesis of $MgCl_2$ films. The main contaminants on this surface are carbon and sulfur. The effective cleaning was achieved at the conditions using Ar pressure $2x10^{-6}$ Torr at the energy of 0.5 keV for sputtering time 15 min and annealing at 500°C for

30 min. After sufficient cycles of Ar^+ sputtering and annealing, these contaminants were completely removed, giving a blur hexagonal LEED pattern. The sharpness of the LEED pattern was hardly improved in spite of a variety of cleaning conditions tested. Au(111) is known to necessarily undergo a peculiar reconstruction during annealing, resulting in a blur hexagonal pattern. According to the imperfectness of the substrate, $MgCl_2$ films grown on Au (111) showed less clear LEED patterns than those on Cu (110). It is notable that Somorjai et al. did not report any LEED patterns for $MgCl_2$ films grown on polycrystalline Au. The thickness of $MgCl_2$ films on Au(111) kept at 303 K was calibrated for the deposition time with the evaporation flux fixed at 20 nA. The film thickness was calculated from the peak attenuation of Au in AES as a function of the deposition time. As shown in Figure 3.14, the film thickness almost linearly increased for the deposition time up to 14 Å, indicating that the sticking probability of impinging $MgCl_2$ molecules is insensitive to the surface coverage. However, the further increase of the thickness caused a severe charging-up problem and the thickness was no longer estimated by AES. The monolayer thickness corresponding to 5.9 Å was achieved approximately at 5.7 min of the deposition.

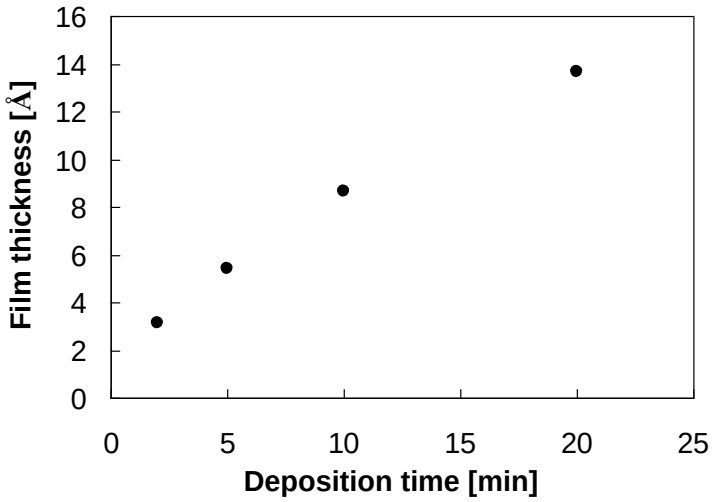

Figure 3.14. The thickness of the $MgCl_2$ film deposited on Au(111) as a function of the deposition time. The flux current was set to 20 nA, and the substrate temperature was held at 303 K.

After careful optimization of the film thickness, a relatively clear hexagonal pattern (corresponding to the appearance of the usual (001) basal plane) was successfully obtained for a monolayer $MgCl_2$ film, as shown in Figure 3.15. The lattice constant estimated from the picture is around 3.6 Å, similar to the monolayer $MgCl_2$ films on Cu (110).

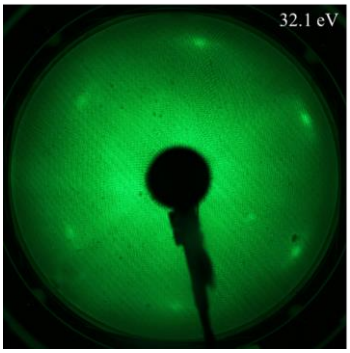

Figure 3.15. LEED pattern of a monolayer $MgCl_2$ film deposited on Au(111)

The packing of $MgCl_2$ units is dominated by $MgCl_2$-$MgCl_2$ interaction to expose the most stable (001) surface. The rotation and lattice constant of the $MgCl_2$(001) surface are decided by the symmetry of underlying substrates.

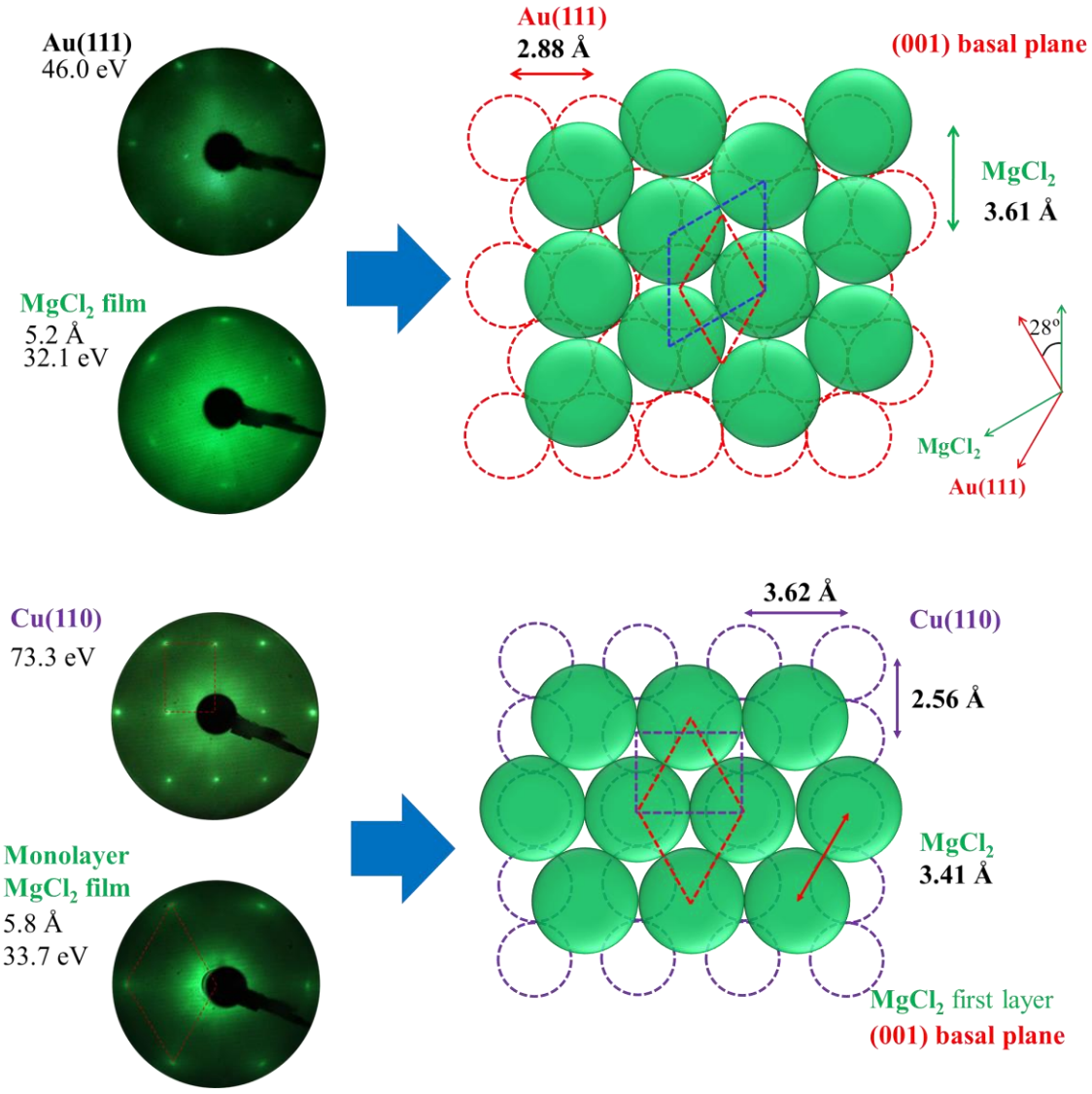

Figure 3.16. Plausible illustrations of the observed LEED patterns of monolayer $MgCl_2$ on substrates

3.3.4 TPD experiments for as-deposited $MgCl_2$ films

Thermal desorption profile of $MgCl_2$ films on Cu(110) substrate was recorded with QMS, monitored at 59 a.m.u ($MgCl^+$). A series of $MgCl_2$ films with different thicknesses were prepared by varying the deposition time from 2.5 min to 40 min at the constant flux of 20 nA. Figure 3.17 shows TPD profiles of the prepared $MgCl_2$ films, where the ramping rate was set at 60 ^oC/min. The desorption of the $MgCl_2$ films always started at around 360 ^oC (leading edge) irrespectively of the film thickness, while the peak-top temperature increased as the film thickness increased (from 404 ^oC for 2.5 min to 457 ^oC for 40 min. The observed desorption temperatures were slightly higher than 380-400 ^oC reported for $MgCl_2$ films over Pt(111), Pd(111), Pd (100) and Rh(111),[1] while lower than 550 ^oC reported for $MgCl_2$ films over polycrystalline Au.[2] Repetitive TPD experiments for the $MgCl_2$ film deposited for 20 min proved good reproducibility in the present TPD/QMS system.

The peak area of the $MgCl_2$ desorption was found to be well proportional to the deposition time and to the film thickness measured by Auger electron spectroscopy (AES) (Figure 3.18). This fact enabled us to estimate the film thickness over 20 Å with TPD/QMS, while AES failed to estimate the correct film thickness over 20 Å due to the charge-up problem.

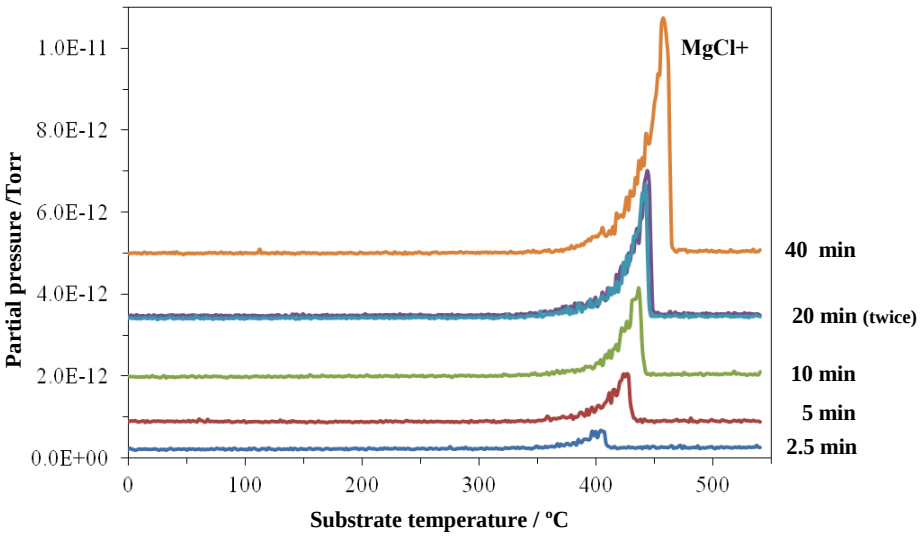

Figure 3.17. TPD profiles at 60 °C/min for $MgCl_2$ films with various thicknesses deposited over Cu(110) substrate.

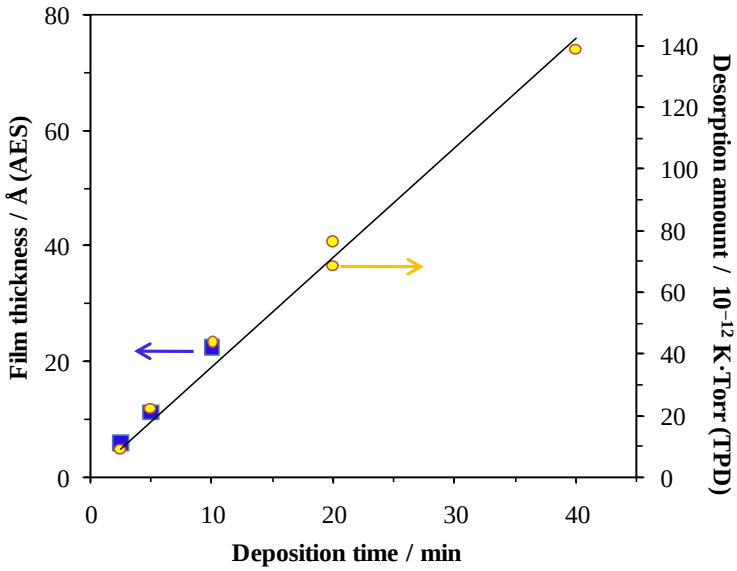

Figure 3.18. Dependence of the film thickness (determined by AES) and the desorption amount (determined by TPD) on the $MgCl_2$ deposition time

3.3.5 TPD experiments for $MgCl_2$ films exposed to Pyridine at different conditions

In order for us to repeatedly investigate the effects of organic molecules using well-controlled $MgCl_2$ films, Pyridine (Py) was chosen for the test organic molecule, not only due to its versatility in surface science study, but also due to its strong coordination ability (~ 30 kcal/mol) to active $MgCl_2$ surfaces. Purified pyridine was degassed using Freeze-Pump-Thaw cycles prior to the introduction to the system. QMS scan over the range of 1 to 100 a.m.u. showed the presence of pyridine-originated mass fragments (such as 26, 39, 52 and 79), whose intensities were proportional to the dose pressure (Figure 3.19).

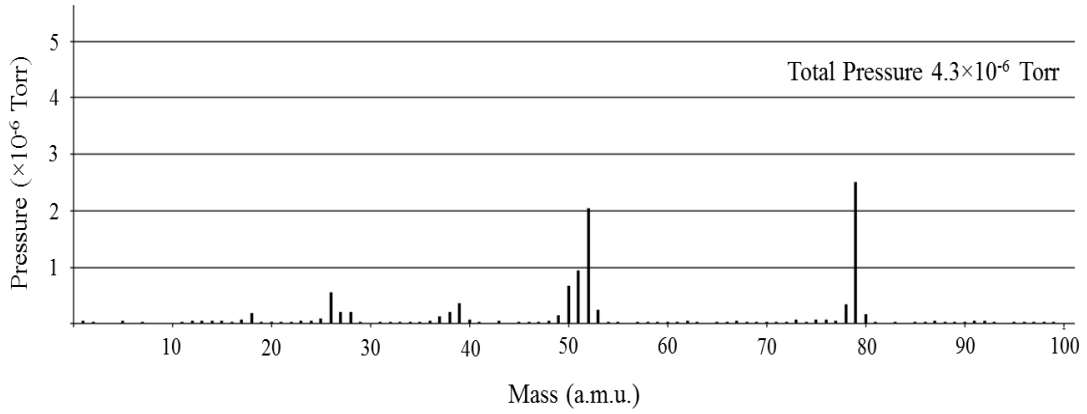

Figure 3.19. Mass spectrum during the introduction of pyridine

First, the Py desorption from Cu(110) substrate was confirmed. The Cu(110) substrate kept at room temperature was exposed to Py at 2.9 Torr (the saturation vapor pressure) for 100 min, and

then subjected to a TPD/QMS experiment. In Figure 3.20, a broad desorption peak of Py was observed over 300 ^{o}C. Since Py never adsorbs on metal surfaces under UHV over room temperature and the desorption peak extended above the decomposition temperature of organic moieties, it was concluded that the observed desorption came from Py molecules adsorbed at a part of the holder, whose temperature was gradually raised as a result of irradiation from the substrate. However, the desorption was not only small enough in intensity but also located sufficiently above the desorption temperature from $MgCl_2$ to neglect it in subsequent experiments.

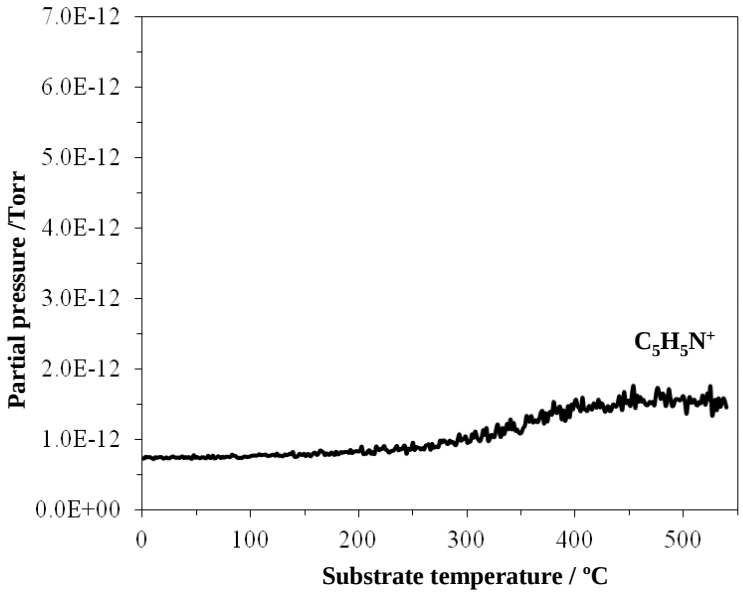

Figure 3.20. TPD profile at 60 ^{o}C/min for Cu(110) substrate exposed to Py at 2.9 Torr for 100 min. Note that the dull desorption peak over 300 ^{o}C is not originated from Cu(110) but from the holder which is indirectly heated by irradiation from the substrate.

Second, $MgCl_2$ films with the thickness of *ca.* 4 nm (corresponding to the deposition time of 20 min) deposited on Cu(110) was exposed to Py vapor at different pressures for 100 min, where the temperature of the substrate was maintained at 100 ^oC. The resultant TPD profiles summarized in Figure 3.21 indicated the significance of the Py pressure on the reconstruction of the $MgCl_2$ film. At the Py pressure of 2 x 10^{-2} Torr, no Py desorption peak was observed, as is the case for previous experiments by Somorjai et al. for the $TiCl_4$ pressure at 10^{-9}-10^{-8} Torr. As-deposited $MgCl_2$ films already exposed the Cl-terminated (001) basal plane over Cu(110) substrate, and these films were chemically and structurally inert. The inertness of the (001) basal plane (against $TiCl_4$) was already known in previous UHV experiments by the other researchers.[15,16] On the other hand, coordinative molecules often make adduct compounds with $MgCl_2$ and can eventually dissolve $MgCl_2$ in powder experiments. We considered that this discrepancy may arise from significantly different concentrations of coordinative molecules between UHV and powder experiments. Therefore, the introduction of coordinative molecules at their saturation vapor pressure was conducted. A Py desorption peak at *ca.* 150 ^oC appeared only when Py pressure was increased above 1.0 Torr. This new desorption peak was assigned to Py species chemisorbed on and/or in the $MgCl_2$ film. The appearance of the Py desorption peak necessarily indicates the reconstruction

of the $MgCl_2$ (001) basal plane for the as-deposited $MgCl_2$ film, since the (001) plane does not expose any Lewis acidic sites. A significant difference in the Py desorption amount between at 1.0 Torr and at 2.9 Torr might be attributed to the fact that the reconstruction of $MgCl_2$ is a multi-molecular process.

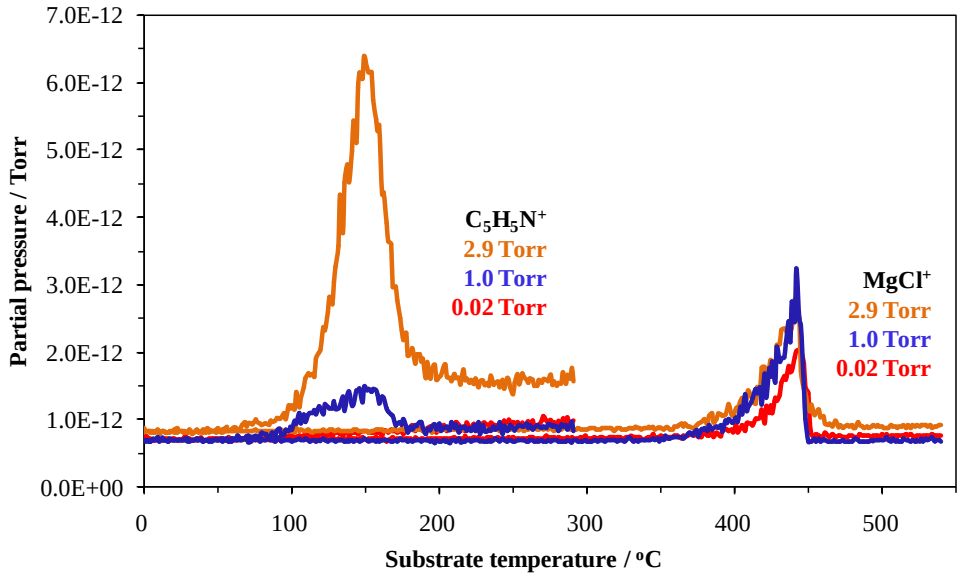

Figure 3.21. TPD profiles at 60 °C/min for $MgCl_2$ films with the thickness of *ca.* 4 nm exposed to Py vapor at various pressures for 100 min.

We have also examined the time dependence of the Py adsorption and resultant $MgCl_2$ reconstruction by changing the exposure time at the Py pressure of 2.9 Torr. TPD profiles in Figure 3.22 showed that the Py adsorption and $MgCl_2$ reconstruction was already equilibrated after 10 min of the exposure.

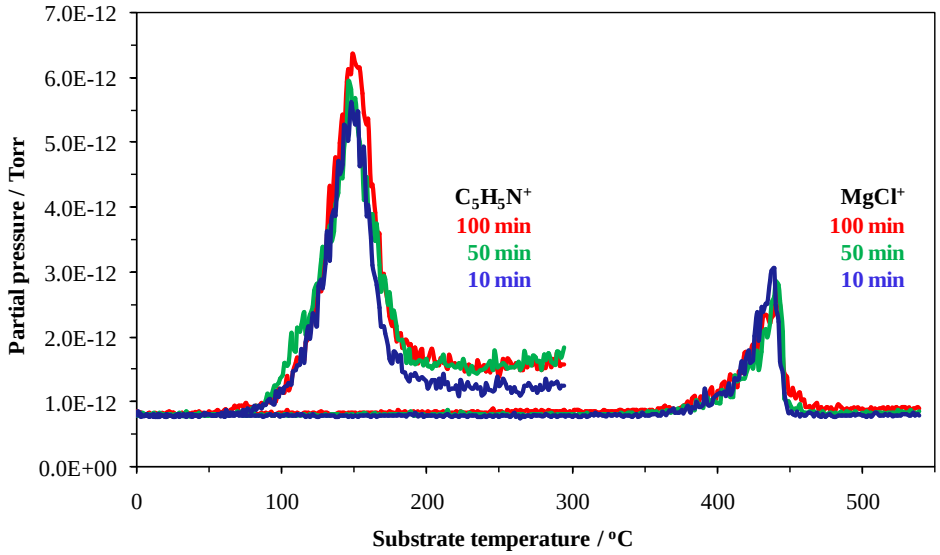

Figure 3.22. TPD profiles at 60 °C/min for $MgCl_2$ films with the thickness of *ca.* 4 nm exposed to Py vapor at 2.9 Torr for different durations.

$MgCl_2$ films with three different thicknesses were exposed to Py vapor at the pressure of 2.9 Torr for 100 min. The Py desorption peak appeared at the same position irrespectively of the film thickness, but the desorption amount was proportional to the film thickness. These results suggest that the Py chemisorption and film reconstruction occurred in the bulk rather than on the film surface, which let us presume the formation of $MgCl_2 \cdot (Py)_n$ adduct.

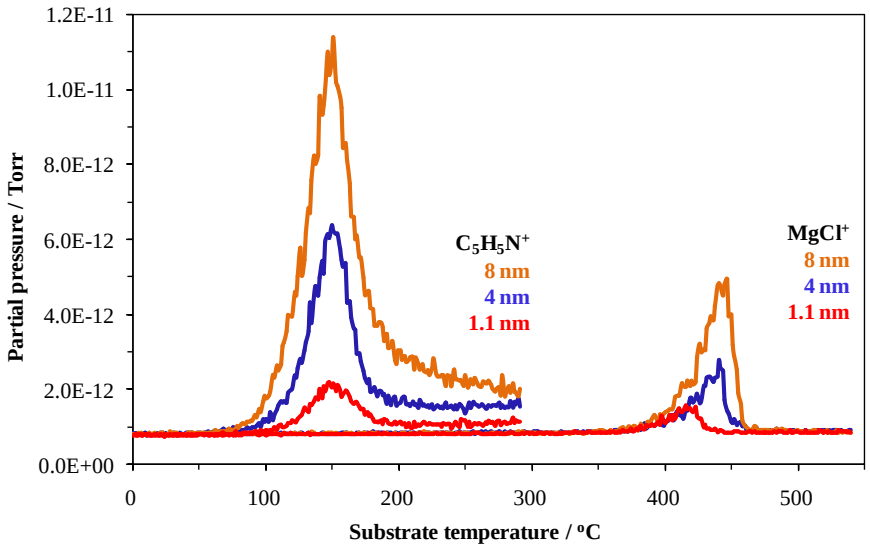

Figure 3.23. TPD profiles at 60 °C/min for $MgCl_2$ films with different thicknesses exposed to Py vapor at 2.9 Torr for 100 min.

3.3.6 LEED experiments for monolayer $MgCl_2$ films exposed to Py

A $MgCl_2$ film with a monolayer-level thickness (11.2 Å) was deposited on the Cu(110) substrate and exposed to Py vapor at 2.9 Torr for 50 min. Figure 3.24 summarizes the alternation of the LEED pattern. The LEED pattern of the as-synthesized $MgCl_2$ film was hexagonal, indicating the exposure of the $MgCl_2$ (001) basal plane Figure 3.24b). After the adsorption of Py and film reconstruction, the LEED pattern changed into a *c*(2 x 1) pattern (Figure 3.24c), which can be explained by a distorted hexagonal Cl placement extended along the [11$\bar{0}$] direction of the substrate (illustrated in Figure 3.24). In this way, the structure of the monolayer Py/$MgCl_2$ film followed

the symmetry of the substrate. However, it must be mentioned that a multi-layer Py/$MgCl_2$ film does not necessarily have the same structure, since the contribution of the substrate-adsorbate interaction becomes negligible.

Next, the monolayer film exposed to Py was annealed at 60 ^{o}C/min up to 180 ^{o}C and then held at 180 ^{o}C for 10 min. As can be seen from Figure 3.26a, the same desorption peak of Py appeared at 150 ^{o}C, even though the $MgCl_2$ film was as thin as monolayer. A separate TPD experiment for the annealed film (Figure 3.24b) confirmed the complete Py removal as a result of the annealing at 180 ^{o}C for 10 min. Interestingly, the LEED pattern of the annealed film still retained the *c*(2 x 1) pattern (Figure 3.24d), even though the Py molecules which had caused the reconstruction did not exist in the film anymore. It is expected that the annealed film remains coordinative vacancies for the adsorption of other molecules such as $TiCl_4$. On the other hand, when the film was annealed at 300 ^{o}C for 10 min rather close to the desorption temperature of $MgCl_2$, the original hexagonal pattern for the (001) basal plane was recovered (Figure 3.24e).

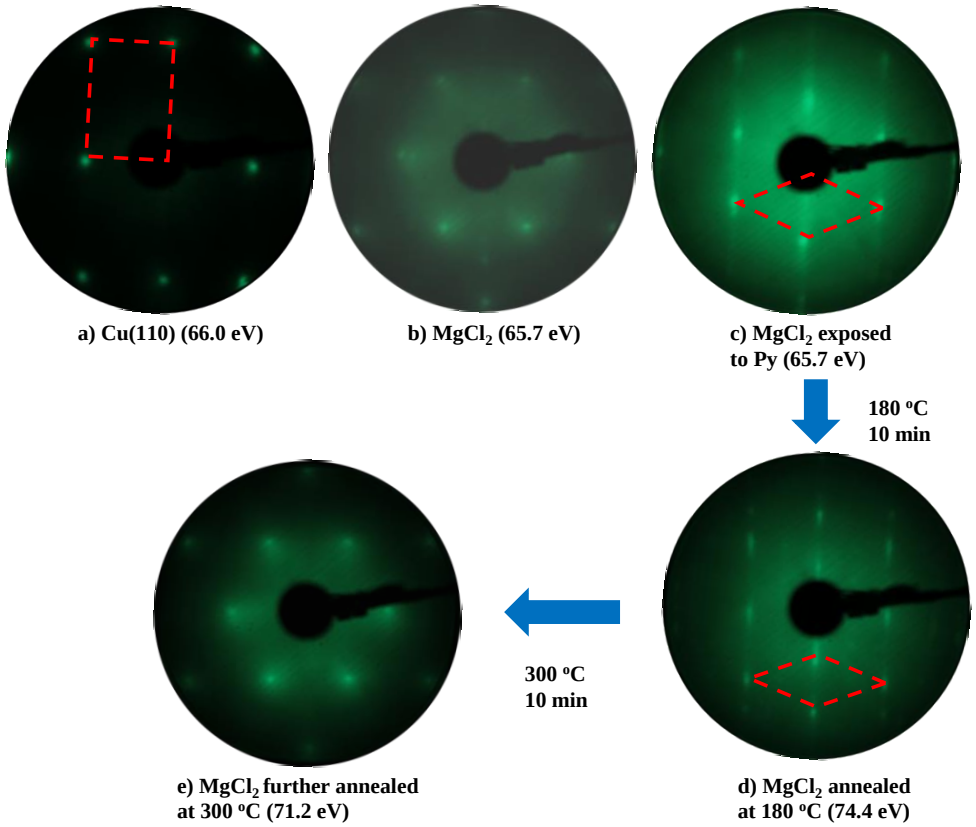

Figure 3.24. LEED patterns of a) Cu(110) substrate, b) as-synthesized monolayer $MgCl_2$ film, c) $MgCl_2$ film after being exposed to Py vapor at 2.9 Torr for 50 min at 100 ^{o}C, d) $MgCl_2$ film after being annealed at 180 ^{o}C for 10 min, and e) $MgCl_2$ film after being further annealed at 300 ^{o}C for 10 min.

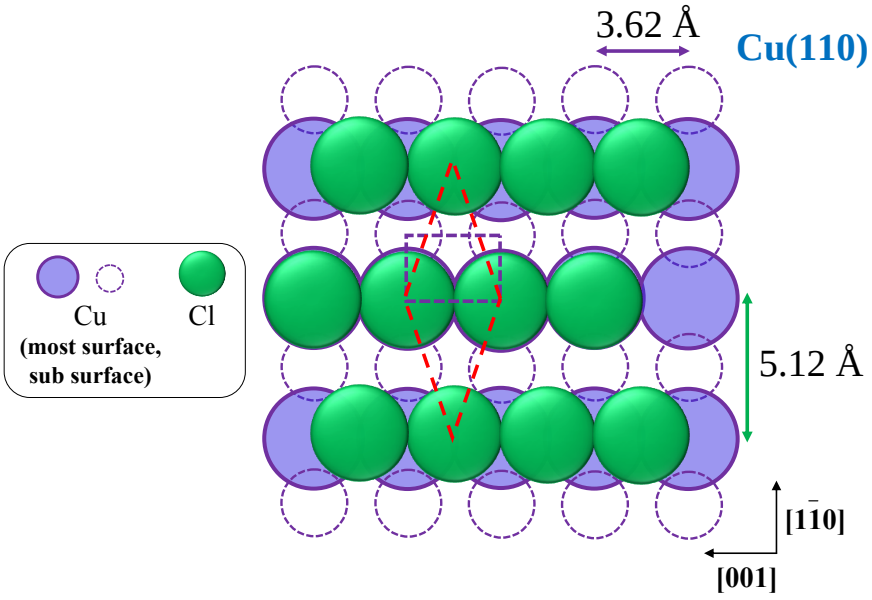

Figure 3.25. Plausible illustration of the observed *c*(2 x 1) structure.

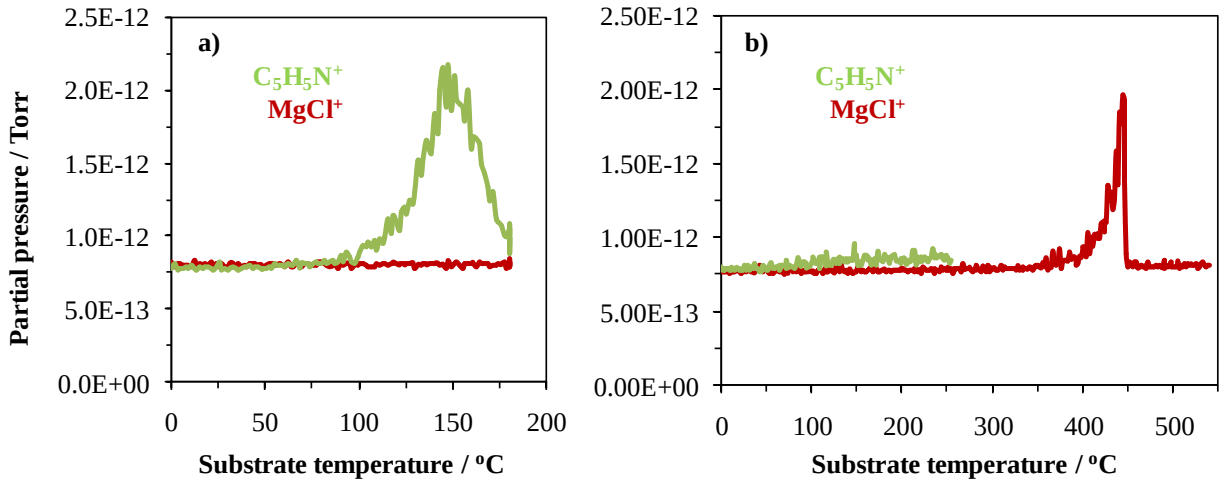

Figure 3.26. TPD profiles at 60 °C/min for a monolayer $MgCl_2$ film exposed to Py vapor at 2.9 Torr for 50 min (up to 180 °C), and for the film pre-annealed at 180 °C for 10 min.

3.3.7 Calculation of desorption energy of Py from $MgCl_2$ films

TPD profiles of $MgCl_2$ films with three different thicknesses exposed to Py vapor at the pressure of 2.9 Torr for 100 min are shown in Figure 3.23. The temperature of peak maximum, T_{max}, is almost constant with coverage indicating that the desorption of Py from $MgCl_2$ film takes place with the first order. Three methods have been applied to calculate the desorption energy of Py from the $MgCl_2$ films: Redhead method, Chan-Aris-Weinberg (CAW) method, and leading edge analysis developed by Habenschaden and Kupper, so-called HK method.

The Redhead method is the simplest and most popular method, which calculates desorption energy from only the T_{max} as shown in equation (1).[20] The pre-exponential factor v was chosen to be 10^{13} s^{-1}, a typical value of choice. In the second popular CAW method, desorption energy is calculated from the T_{max} and the peak width at haft of maximum intensity (W) as shown in equation (2).[21] In the leading edge analysis based on Arrhenius plot of desorption spectrum in a small temperature interval at low-temperature side, where the variation of temperature and coverage are slightly small. It is easily derived from Polanyi-Wigner equation that $-E_{des}(\theta)/R$ is the slop of this strait line.[22] Results of Py desorption energy from $MgCl_2$ films calculated with three methods are summarized in Table 1.

$$E_{des} = RT_{\max}\left[\ln\left(\frac{\nu T_{\max}}{\beta}\right) - 3.46\right] \quad \text{Eq. (1)}$$

$$E_{des} = RT_{\max}\left[-1 + \sqrt{1 + 5.832\left(\frac{T_{\max}}{W}\right)^2}\right] \quad \text{Eq. (2)}$$

$$\ln\left(-\frac{\mathrm{d}\theta}{\mathrm{d}t}\right) = \ln\nu(\theta) + n \cdot \ln\theta + \left(\frac{-E_{des}}{R}\right)\frac{1}{T} \quad \text{Eq. (3)}$$

Where E_{des}: activation energy of desorption ($J \cdot mol^{-1}$)

R: gas constant (8.314 $J \cdot mol^{-1} \cdot K^{-1}$)

T_{max}: temperature at peak maximum (^oC)

v: pre-exponential factor (s^{-1})

β: heating rate ($^oC \cdot s^{-1}$)

W: peak width at haft maximum (^oC)

Table 1. desorption energy of Py from $MgCl_2$ films calculated with three methods

Film thickness (Å)	E_{des} (kcal·mol^{-1})		
	Redhead	CAW	HK
1.1	27.2	19.4	8.8
4	27.3	24.4	10.7
8	27.4	23.1	12.2

Desorption energy calculated by Redhead and CAW methods, which are coverage independent, are reasonable for the existence of Py under UHV conditions. The lower desorption energy of the 1.1 Å film calculated with CAW method comes from the low quality of TPD result. It is interesting that the desorption energy values obtained with the Redhead method are comparable with adsorption energy of Py on different $MgCl_2$ faces calculated by DFT calculation. The leading edge analysis gave small desorption energy values, which are not suitable for the existence of Py under UHV conditions. Increase of the desorption energy with coverage indicates this method is not suitable for calculating desorption energy of Py from $MgCl_2$ film.

3.3.7 Calculation of desorption energy of Py from $MgCl_2$ films

$MgCl_2$ was deposited on the clean Cu(110) substrate for 20 min at the emission current of 10 mA, which corresponded to the $MgCl_2$ film thickness of *ca.* 4 nm. The reproduction of the $MgCl_2$ deposition was confirmed by the temperature programmed desorption (TPD). The prepared $MgCl_2$ film kept at 100°C was exposed to pyridine (Py) at 1.0 or 2.9 Torr for 100 min in a separate chamber equipped with a Py dosing line and liquid N_2 trap. The resultant films were subjected to TPD experiments at the ramping rate of 60°C/min (Figure 3.27). A desorption peak for Py appeared around 150°C only in the presence of a $MgCl_2$ film, whose intensity was sensitive to the Py pressure (and proportional to the $MgCl_2$ film thickness). The broad peak indicates coverage-dependent desorption energy and the average desorption energy was estimated to be 24-27 kcal/mol. On the other hand, the desorption peak for $MgCl_2$ was unaffected by Py in its position and intensity. This is because the film structure is reconstructed into that of the original (001) surface at least at 300°C. Thus, most of our findings were successfully reproduced after repairing the electron gun. However, TPD experiments shown in Figure 3.24 pose one difference from the Figure 3.23 data, that is, the peak intensity for $C_5H_5N^+$ (m/z = 79) was several times smaller than those reported in Figure 3.23. Instead, the peak intensity for $C_4H_4^+$ (m/z = 59), the main fragment,

became much higher than that for $C_5H_5N^+$. In general, fragments are formed as a result of decomposition of a main mass on the filament. Though it was thought that the status of the filament might be changed.

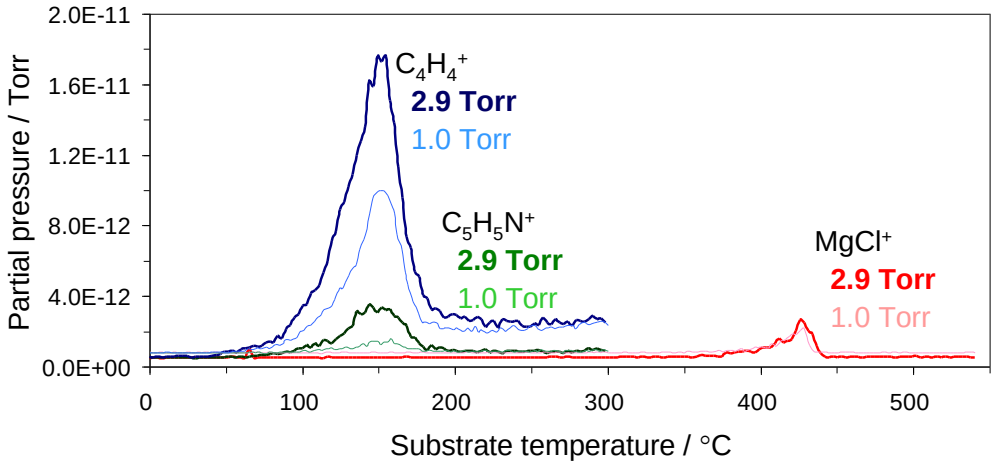

Figure 3.27. TPD profiles at 60 °C/min for $MgCl_2$ films with the thickness of *ca.* 4 nm exposed to Py vapor at 1.0 and 2.9 Torr for 100 min.

3.3.8 Re-adsorption of Py on a 4 nm-thick $MgCl_2$ film

We had reported that when a 1-nm-thick $MgCl_2$ film was exposed to 2.9 Torr of Py, the low energy electron diffraction (LEED) pattern of the film transformed from hexagonal to *c*(2x1), while the *c*(2x1) pattern remained even after the removal of Py at 180°C. It had been supposed that the $MgCl_2$ film left after the Py removal might keep some active structure, which might allow the adsorption of molecules even at a low pressure. To answer this hypothesis, the following

experiments were conducted. Firstly, a 4-nm-thick $MgCl_2$ film was prepared on Cu(110) by the $MgCl_2$ deposition for 20 min. The film was then exposed to 2.9 Torr of Py for 20 min at 100°C, followed by the Py removal at 180°C with the TPD apparatus. Thereafter, the film was again exposed to 500 mTorr of Py for 20 min at 100°C. Finally, the amount of Py re-adsorbed in the film at the reduced pressure was examined with the TPD experiment.

Figure 3.28 summarizes the results of the re-adsorption experiments. When as-deposited films were exposed to Py, the Py pressure was critically important for the amount of adsorbed Py (compare 2.9 Torr, 1st with 500 mTorr, 1st). Unfortunately the same conclusion held for the 2nd adsorption: The amount of re-adsorbed Py was almost the same as that for the direct exposure at the same pressure (500 mTorr, 2nd vs. 500 mTorr, 1st). In this way, the 4-nm-thick $MgCl_2$ film exhibited the repeatable adsorption and desorption of Py molecules, rather than keeping an active structure after the removal of Py at 180°C.

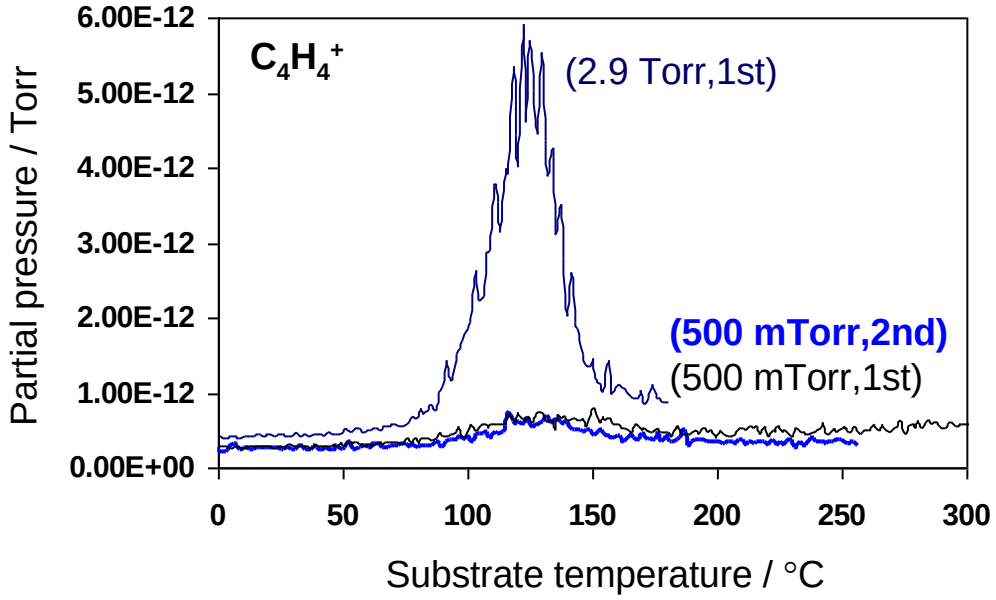

Figure 3.28. TPD spectra for Py re-adsorption experiments on a 4-nm-thick $MgCl_2$ film. The film once exposed to 2.9 Torr of Py was subjected to an TPD experiment up to 180°C (2.9 Torr, 1st), and then re-exposed to 500 mTorr of Py (500m Torr, 2nd). For comparison, the TPD spectrum for a film exposed to 500 m Torr of Py (500 mTorr, 1st) is also shown.

It was envisaged that the above-mentioned hypothesis might hold only for a monolayer-level film, whose structure might be fixed by the Cu(110) substrate. On the other hand, a thick $MgCl_2$ film might not have a driving force to keep a defective structure left after the Py removal. Therefore, the same experiments are now ongoing for a 1-nm-thick film.

3.3.9 Re-adsorption of Py on a 1 nm-thick $MgCl_2$ film

The same re-adsorption experiment for 1 nm-thick $MgCl_2$ film was conducted (Figure 3.29). Monolayer-level film might retain coordinative vacancies even after the Py desorption. In detail, 1 nm-thick $MgCl_2$ film deposited on clean Cu(110) was exposed to 2.9 Torr of Py at 100°C for 20 min to prepare Py/$MgCl_2$ film. Adsorbed Py was removed by heating the substrate at 180°C for 10 min. In our previous LEED study, the film left after the Py desorption kept a *c*(2x1) surface structure. The film was re-exposed to 500 mTorr of Py at 100°C for 20 min, and then subjected to an TPD experiment at 60 °C/min. As was concluded for 4 nm-thick $MgCl_2$ film, it was found that the Py adsorption amount was invariant between the reconstructed film (left after the Py removal) and the as-deposited film at a given pressure (500 mTorr). Busico has mentioned that $MgCl_2$ behaves like a living material, readily adapting its structure to a given environment. Our findings are exactly in the same line with this idea: $MgCl_2$ film adapted its structure to the environment of 500 mTorr of Py at 100°C, while the film kept the reconstructed *c*(2x1) structure in the absence of Py. Thus, a new aspect can be added to the Busico's idea that the presence of strong Lewis bases kinetically accelerates the structural equilibration of $MgCl_2$.

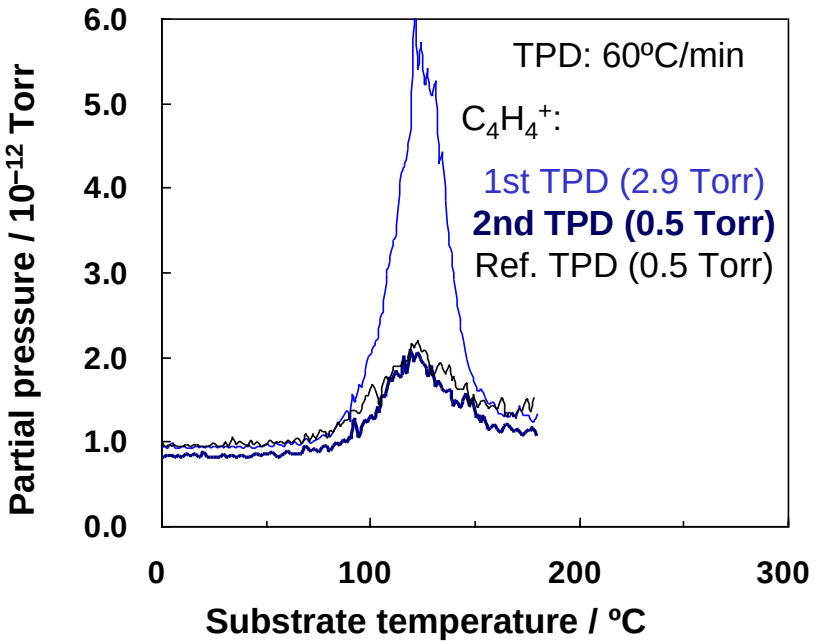

Figure 3.29. TPD spectra for Py re-adsorption experiments on 1 nm-thick $MgCl_2$ film. The film once exposed to 2.9 Torr of Py was subjected to an TPD experiment up to 180°C (2.9 Torr, 1st), and then re-exposed to 500 mTorr of Py (500m Torr, 2nd). For comparison, the TPD spectrum for a film exposed to 500 m Torr of Py (500 mTorr, 1st) is also shown.

3.3.10 Adsorption of other donors

4 nm-thick $MgCl_2$ film was exposed to tetrahydrofuran (THF) or ethylbenzoate (EB) at different conditions. THF was purified over Na and then with pump-and-thaw cycles. EB was purified over molecular sieve 4A and then with intensive pump-and-thaw cycles. Figure 3.30 summarizes TPD profiles obtained from 4 nm-thick $MgCl_2$ film exposed to 2.9 or 4.2 Torr of THF at 50°C for 20 min, where $C_3H_6^+$ (m/z=42) was tracked as the main fragment of THF. Interestingly, THF

hardly adsorbed onto the $MgCl_2$ film at 2.9 Torr, while a large amount adsorbed at the same pressure in the case of Py. The pressure required to promote the THF adsorption was 4.2 Torr, nearly its saturated vapor pressure. Judging from the least pressures to enable significant adsorption of Py and THF, it was concluded that the reconstruction of (001)-terminated $MgCl_2$ film necessitates the presence of donors at their own saturated vapor pressure.

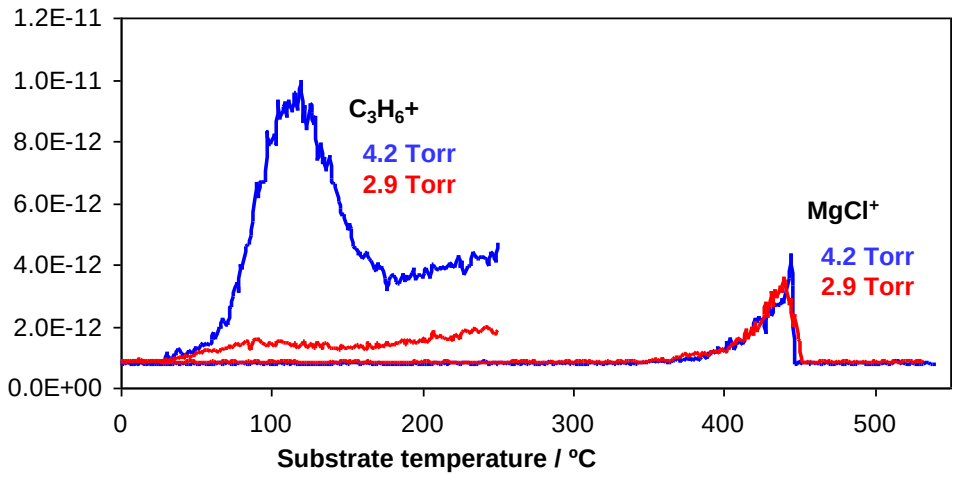

Figure 3.30. TPD profiles of 4 nm-thick $MgCl_2$ film after being exposed to 2.9 or 4.2 Torr of THF at 50°C for 20 min

Next, 4 nm-thick $MgCl_2$ film was similarly exposed to 400 mTorr of EB (the saturated pressure) at 90°C for 6 h. As can be seen in Figure 3.31, we could not observe any adsorption of EB. The situation was unchanged irrespective of the substrate temperature and exposure time. In powder experiments, EB can dissolve $MgCl_2$ much less compared with Py and THF. Since the adsorption

strength of EB on $MgCl_2$ is more or less similar to those of Py and THF, the observed difference in reconstructing $MgCl_2$ film and in dissolving $MgCl_2$ powder must be attributed to the bulkiness of EB, which not only decelerates the molecular penetration but also lowers the maximum number of molecules that can coordinate per $MgCl_2$.

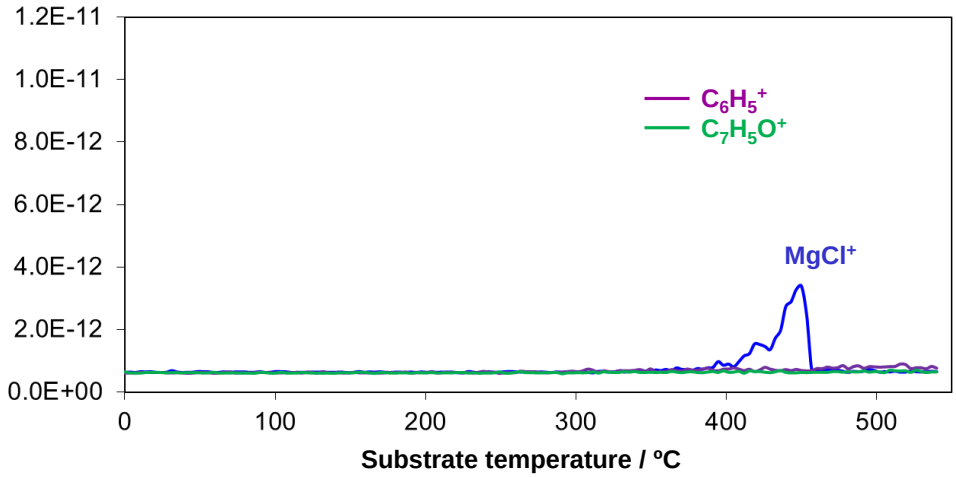

Figure 3.31. TPD profiles of 4 nm-thick $MgCl_2$ film after being exposed to 400 mTorr of EB at 90°C for 6 h

3.4 Conclusion

We have clarified that $MgCl_2$ readily adapts its structure to the environment in the presence of strong Lewis bases, the saturated vapor pressure of a donor is essential to cause the reconstruction of (001)-terminated $MgCl_2$ film, and the ability of a donor to reconstruct $MgCl_2$ film can be considered in relation to the ability of the donor to dissolve $MgCl_2$ powder. Obtained $MgCl_2$ film is a promising precursor toward the preparation of realistic Ziegler-Natta model surfaces in UHV.

References

[1] V. Busico, P. Corradini, L. De Martino, A. Proto, V. Savino. E. Albizzati, *Makromol. Chem.* **1985,** *186*, 1279.

[2] L. Brambilla, G. Zerbi, F. Piemontesi, S. Nascetti, G. Morini, *J. Mol. Catal. A: Chem*. **2007**, *263*, 103.

[3] T. Taniike, M. Terano, *J. Catal*. **2012**, *293*, 39.

[4] M. D'Amore, R. Credendino, P.H.M. Budzelaar, M. Causà, V. Busico, *J. Catal*. **2012**, *286*, 103.

[5] V. Busico, R. Cipullo, G. Monaco, G. Talarico, M. Vacatello, J.C. Chadwick, A.L. Segre, O. Sudmeijer, *Macromolecules* **1999**, *32*, 4173.

[6] A. Correa, F. Piemontesi, G. Morini, L. Cavallo, *Macromolecules* **2007**, *40*, 9181.

[7] A. Andoni, J.C. Chadwick, J.W. Niemantsverdriet, P.C. Thüne, *J. Catal.* **2008**, *257*, 81.

[8] R. Credendino, J.T.M. Pater, A. Correa, G. Morini, L. Cavallo, *J. Phys. Chem. C* **2011**, 115, 13322.

[9] E. Magni, G.A. Somorjai, *Appl. Surf. Sci.* **1995**, *89*, 187.

[10] E. Magni, G.A. Somorjai, *Surf. Sci.* **1995**, *341*, 1078.

[11] H.-J. Freund, M. Bäumer, J. Libuda, T. Risse, G. Rupprechter, and S. Shaikhutdinov, *J. Catal.* **2003**, *216*, 223.

[12] D. H. Fairbrother, J. G. Roberts and G. A. Somorjai, Surface Science **1998**, *399*, 109.

[13] D. H. Fairbrother, J. G. Roberts, S. Rizzi and G. A. Somorjai, Langmuir **1997**, *13*, 2090.

[14] F. Reinert, G. Nicolay, Appl. Phys. A **2004**, *78*, 817.

[15] E. Magni, G. A. Somorjai, J. Phys. Chem, **1996**, *100*, 14786.

[16] T. Risse, J. Schmidt, H. Hamann, H. J. Freund, Angew. Chem. Int. Ed., **2009**, *41*, 1517.

[17] G. S. Rohrer, V. E. Henrich, D. A. Bonnell, *Science*, **1990**, *250*, 1239.

[18] H. Onishi, K. I. Fukui, Y. Iwasawa, *Bull. Chem. Soc. Jpn.*, **1995**, *68*, 2447.

[19] U. Diebold, *Surf. Sci. Rep.*, **2003**, ***48***, 53.

[20] P. A. Redhead, *Vacuum*, **1962**, *12*, 203.

[21] C. M. Chan, R. Aris, W. H. Weinberg, *Appl. Surf. Sci.*, **1978**, *1*, 360.

[22] E. Habenschaden, J. Kupper, *Surf. Sci.*, **1984**, *138*, L147.

Chapter 4

General Conclusions

4.1 General Summary

This dissertation discussed about development Ziegler-Natta model catalyst The results obtained are summarized as below.

In Chapter 1, polyolefin polymerization catalysts, structure and chemistry of $MgCl_2$-supported catalysts, current understanding of Ziegler-Natta (model) catalysts were introduced as general introduction for the purpose of leading the objective this dissertation.

In Chapter 2, the active site natures of various $MgCl_2$-supported cyclopentadienyl Ti chloride catalysts were systematically investigated and compared with traditional catalysts. Polymerization properties and active site formation of these catalysts were investigated. The supported titanocene catalysts offered both metallocene-type and Ziegler-Natta-type active site natures according to the details of the preparation and the activation procedures. The observed dual active site natures were plausibly correlated with the valence and charge states of the Ti center.

In Chapter 3, the purpose is that UHV Synthesis and characterization of $MgCl_2$ active surfaces prepared by donor-induced surface reconstruction. $MgCl_2$ film deposited on single-crystal metal substrates always exposes the (001) surface irrespective of their surface symmetry, which does not allow the adsorption of donors under usual UHV conditions. $MgCl_2$·donor adducts are formed

when $MgCl_2$ film is exposed to the vapor of a donor at a nearly saturated vapor pressure. While the desorption of a donor at a mild temperature leaves coordinative vacancies for $MgCl_2$ film, the introduction of a donor readily reconstruct the film structure into equilibrated one at a given environment (temperature, pressure). Thus, $MgCl_2$ structure is highly flexible in the presence of coordinating molecules, which seems to kinetically accelerate the reconstruction of $MgCl_2$.

4.2 General conclusion

Research about the nature of Ziegler-Natta catalysts is ongoing because of the industrial importance for development of new grades of PP. However, despite extensive efforts, there is still limited understanding of the nature of Ziegler-Natta catalysts, especially this is because the nature of active sites. Using model catalysts which can reduce heterogeneity is one of the helpful ways to address problems of the multisite nature. In this study, we found novel dual active site natures of $MgCl_2$-supported titanocene catalysts, which can be switched by the kind of activator. The role of $MgCl_2$ is to stabilize the reduced Ti species as isospecific active sites. Moreover, a synthetic route for active $MgCl_2$ surfaces has been established by donor-induced reconstruction in UHV experiments. Obtained $MgCl_2$ film is a promising precursor toward the preparation of realistic Ziegler-Natta model surfaces in UHV. The results in this study are remarkably important for

development of useful model catalyst. The knowledge obtained in this study will contribute to the further development of the $MgCl_2$-supported Ziegler-Natta catalysts and the unique materials with improved properties.

Achievements

Publications

Original Articles

K. Goto, T. Taniike, M. Terano, Dual-Active-Site Nature of Magnesium Dichloride-Supported Cyclopentadienyl Titanium Chloride Catalysts Switched by an Activator in Propylene Polymerization, *Macromol*. *Chem*. *Phys*. **2013**, *214*, 1011-1018.

Presentations

International Conferences

Propylene Polymerization with Ziegler–Natta Model Catalysts Having $MgCl_2$-Supported Titanocene

K. Goto, T. Taniike, M. Terano

Advances in Polyolefins 2011, Santa Rosa, USA, Sep. 25-28, 2011.

Propylene Polymerization with $MgCl_2$-Supported Titanocene Catalysts as a Model of Ziegler–Natta Catalysts

K. Goto, T. Taniike, M. Terano

8 th International Colloquium on Heterogeneous Ziegler-Natta Catalysts, Ishikawa, Japan, Mar. 27-30, 2012.

Ligand Effects for Active Site Formation of $MgCl_2$-supported Titanocene Catalysts

K. Goto, T. Taniike, M. Terano

International Conference on the Reaction Engineering of Polyolefins, Ferrara, Italy, Sep. 2-5, 2013

Domestic Conferences

Influences of cyclopentadienyl ligands on propylene polymerization properties of $MgCl_2$-supported titanium chloride catalysts

K. Goto, S. Takahashi, T. Taniike, M. Terano

59th SPSJ Annual Meeting, Yokohama, May 26-27, 2010.

Preparation and Active Site Formation of Supported Titanocene Ziegler–Natta Model Catalysts

K. Goto, S. Takahashi, T. Taniike, M. Terano

59th SPSJ Symposium on Macromolecules, Sapporo, Sep 15-17, 2010.

Influences of ligands and oxidation states for Ziegler–Natta model catalysts synthesized with Titanocene complexes

K. Goto, S. Takahashi, T. Taniike, M. Terano

60th SPSJ Annual Meeting, Osaka, May 28-30, 2011.

Control of active site structure and olefin polymerization properties of $MgCl_2$-supported titanocene catalysts by activator

K. Goto, T. Taniike, M. Terano

61th SPSJ Annual Meeting, Yokohama, May 29-31, 2012.

UHV preparation of $MgCl_2$ active surface for Ziegler-Natta catalyst

K. Goto, T. Taniike, M. Terano

62th SPSJ Symposium on Macromolecules, Ishikawa, Sep 11-13, 2013.